

In situ $\delta^{13}\text{C}$ and $\delta^{18}\text{O}$ microanalysis by SIMS: A method for characterizing the carbonate components of natural and engineered CO₂-reservoirs



Maciej G. Śliwiński ^{a,*}, Kouki Kitajima ^a, Reinhard Kozdon ^{a,b}, Michael J. Spicuzza ^a, Adam Denny ^a, John W. Valley ^a

^a WiscSIMS, Department of Geoscience, University of Wisconsin-Madison, Madison, WI 53706, United States

^b Lamont-Doherty Earth Observatory of Columbia University, Palisades, NY 10964, United States

ARTICLE INFO

Article history:

Received 1 June 2016

Received in revised form

13 December 2016

Accepted 19 December 2016

Available online 10 January 2017

Keywords:

Carbon sequestration

Natural analogues

Carbonate cements

Carbon isotopes

SIMS microanalysis

Illinois Basin

Illinois Basin Decatur Project

ABSTRACT

This work addresses the potential utility of *in situ* carbon and oxygen isotope microanalysis ($\delta^{13}\text{C}$ and $\delta^{18}\text{O}$) by secondary ion mass spectrometry (SIMS) in carbon sequestration research. A desirable long-term consequence of CO₂-injection into underground rock formations at prospective sequestration sites (such as deep saline sandstone aquifers capped by impermeable strata) is the precipitation of carbonate mineral cements, the isotopic fingerprinting of which is a central theme here. More specifically, we focus on the unique advantage of the SIMS technique, which lies in the capability of analyzing very small sample volumes that are otherwise inaccessible to sampling techniques in conventional isotope ratio mass spectrometry (IRMS). For example, single carbonate crystallites as small as 3–10 μm across can be readily analyzed by SIMS with sub per-mil (‰) accuracy and precision. Importantly, the ability to perform micrometer-scale measurements *in situ* from either thin sections or 1-in. (25 mm) diameter polished core plugs preserves the petrographic context of measured carbonate $\delta^{18}\text{O}$ and $\delta^{13}\text{C}$ values.

We provide a preliminary characterization of the pre-injection mineralogy and isotopic fingerprints of carbonate cements in the Mount Simon Sandstone reservoir and the overlying silty-shaly caprock (the Eau Claire Formation) at the Illinois Basin Decatur Project, a demonstration and research site for exploring the feasibility of long-term CO₂ storage in a deep saline aquifer. By drawing upon published data on ambient reservoir conditions and the isotopic composition of the injected CO₂, we make simple predictions regarding possible $\delta^{13}\text{C}$ values of calcite, dolomite-ankerite, and siderite cements that may form in response to long-term CO₂ storage.

© 2016 Elsevier Ltd. All rights reserved.

1. Introduction

Geological storage of carbon dioxide gas (CO₂) emissions produced by human industrial and agricultural activities is actively being evaluated as a means of mitigating global climate change (e.g., Bachu et al., 1994; Celia et al., 2015; DePaolo and Cole, 2013; DOE, 2010; IPCC, 2005; Lackner et al., 1995; Matter et al., 2016; McGrail et al., 2016; Power et al., 2013). Capturing CO₂ from stationary point sources (e.g., coal-fired power plants) and storing it in geological environments, such as in deep saline aquifers, is a technologically feasible (e.g., Hosa et al., 2011; Michael et al., 2010, 2009) and potentially viable stand-in solution for some time to come

as societies gradually transition to alternative and more sustainable clean energy-producing technologies (e.g., Baines and Worden, 2004a; Bickle, 2009; Celia et al., 2015; Gale, 2004; Hoffert et al., 2002; Lackner, 2003). At present, the large-scale deployment and implementation of this carbon capture and storage (CCS) strategy is seemingly impeded first and foremost by economic inconvenience (e.g., Celia et al., 2015; Gibbins and Chalmers, 2008; Michael et al., 2009; Orr, 2009; Wigley et al., 1996).

An important objective of research efforts concerned with the feasibility of sequestering carbon in a variety of potentially suitable geological environments (e.g., deep saline sandstone aquifers, depleted oil and gas reservoirs, unmineable coal seams, flood basalt provinces or ultramafic rock formations; e.g., Baines and Worden, 2004a; McGrail et al., 2006) is the ability to make realistic predictions about the long-term fate of stored CO₂ (on a time scale exceeding 10,000 years). A recent volume of Reviews in Mineralogy

* Corresponding author.

E-mail address: msliwinski@wisc.edu (M.G. Śliwiński).

and Geochemistry showcases some of the modern techniques and approaches that are being applied in this field of research (DePaolo and Cole, 2013) and outlines the leading geologically-oriented thematic questions. Among others, these include the following: What is the relative importance of different CO₂-trapping mechanisms in different types of prospective reservoirs, and how long are they effective (e.g., structural/stratigraphic or solubility trapping vs. carbon mineralization; Gunter et al., 2004)? What geochemical reactions are likely to occur (and at what rates) between the mineralogy of a given reservoir-caprock system and its waters/brines, which become reactive due to CO₂-charging? What is the capacity for reactions to consume CO₂ and to produce carbonate mineral cements, where in the system are such cements likely to form, and over what time scales are such reactions likely to occur? This process, referred to as carbon mineralization (or mineral trapping of CO₂), constitutes the most secure and effectively permanent form of CO₂ storage.

Much insight into many of the above questions concerning the long-term fate of sequestered CO₂ comes from studies of so called natural analogues, or geological environments where large quantities of CO₂ have accumulated and remained confined over geologic time scales (e.g., Baines and Worden, 2004b; Bickle et al., 2013). Such accumulations exist, for example, in certain deeply-buried permeable sandstone formations (saline aquifers/reservoirs) that are overlain by effectively impermeable sediments that act as seals (or ‘caprocks’, e.g., shales or salt beds; Haszeldine et al., 2005; Heinemann et al., 2013; Lu et al., 2011, 2009; Pearce et al., 1996; Sathaye et al., 2014; Watson et al., 2004; Wilkinson et al., 2009). For a given reservoir-caprock system, studies of natural analogues help to characterize the predominant fluid-mineral reactions that could be reasonably expected during engineered CO₂ storage and allow for estimating rates of carbon mineralization. They further provide a means of ground-truthing (or ‘history-matching’) the results of geochemical models that seek to predict how a particular type of reservoir will evolve in the long-term as its mineralogy is subjected to a CO₂ charge. In this regard, the knowledge gained from natural analogues is indispensable for the simple reason that rates of geochemical reactions are generally not well constrained at the relatively low temperature conditions of many prospective CO₂ storage reservoirs, which severely limits the predictive power of models. Baines and Worden (2004b) make an elegant point in noting that a model generally “tells us how a rock [or given reservoir unit] should evolve to reach thermodynamic equilibrium, not whether it will evolve,” and does not “inform us how long (or even if) a reaction will occur.”

With regards to estimating carbon mineralization rates, a substantial difficulty in natural analogue studies commonly lies in distinguishing carbonate cements that formed in response to natural CO₂-charging from those cements that may have formed during earlier stages of sediment alteration (Heinemann et al., 2013; Wilkinson et al., 2009). In the case of sandstone reservoirs, carbonate minerals are a common cement type (Morad, 2009). Measurements of stable isotope ratios of carbon and oxygen ($\delta^{13}\text{C}$ and $\delta^{18}\text{O}$, respectively) can serve as a useful diagnostic tool; however, drawing distinctions based on the results of conventional sampling techniques in isotope ratio mass spectrometry (IRMS) can be complicated because a thorough mechanical separation of different carbonate cement populations (or sampling of individual zones within single crystals) is often not possible due to small crystal size.

This study aims to demonstrate the applicability in carbon sequestration research of recent advances in the analytical methods of measuring carbon and oxygen isotope ratios in carbonate minerals by secondary ion mass spectrometry (SIMS). This technique allows for micrometer-scale measurements to be made *in situ* from either thin sections or 1-in. diameter core plugs, thus preserving the

petrographic context of analyzed sample volumes (e.g., Śliwiński et al., 2016a,b; Valley and Kita, 2009). To this end, we provide a preliminary characterization of the mineralogy and the isotopic fingerprints of the major existing carbonate cement generations in the upper Mt. Simon Sandstone reservoir and the overlying Eau Claire shale at the Illinois Basin Decatur Project site (IBDP; Fig. 1), where 1 million metric tons of CO₂ have now been successfully injected to demonstrate the technological feasibility of sequestration in a deep saline sandstone reservoir (DOE, 2010; Leetaru et al., 2009; Leetaru and Freiburg, 2014). The technique we describe may more broadly find use as a tool for monitoring the progress of carbonate mineral cement-forming reactions within reservoir-caprock systems, especially during the early post-injection period (years to decades?), when only small volumes of new carbonate will likely be forming. As little as 3 micrometers (μm) of new cement growth could be readily analyzed by SIMS with sub-per mil accuracy and precision, and such data could conceivably be the basis for quantitative, up-scaled reservoir simulations that attempt to predict the eventual volume of CO₂ that may become securely trapped in mineral form. Smaller, nanometer-scale domains can be analyzed using a sub- μm spot (Page et al., 2007) in cases where steep isotopic gradients are suspected.

2. Methods

The sandstone beds examined in this study were collected from the transition zone between the upper unit of the Upper Cambrian Mt. Simon Sandstone and the basal unit of the overlying Eau Claire Fm. from core material recovered from the IBDP Verification Well #1 (Fig. 1), at depths of 1680.4 m (5513.2 ft), 1677.3 m (5502.9 ft), and 1676.8 m (5501.3 ft) (this depth interval corresponds to Unit A of Palkovic (2015) – see Fig. 4.1 therein). Due to sampling restrictions, the overlying Eau Claire Fm. was sampled from core material from a well in a nearby county, ~75 km (~45 miles) to the WSW of IBDP (C13637, at depths of 1096.5 m (3597.5 ft), 1096.7 m (3598 ft) and 1094.8 m (3592 ft); Fig. 1).

Subsamples of core (Fig. 2) were first roughly polished using a series of diamond-embedded abrasive pads (20, 10 and 6- μm) and examined by scanning electron microscopy (SEM; Hitachi S3400-N) to quickly and efficiently locate carbonate-cemented intervals. For this initial examination, the sample surfaces were not coated with a conductive material (e.g., with carbon, Au, Ir, etc.) as is customary for high-resolution imaging, and the SEM was instead operated in variable-pressure mode to reduce the detrimental effects of charging on image quality. Carbonate cements were identified using energy-dispersive x-ray fluorescence spectroscopy (ED-XRF; ThermoFisher detector coupled to SEM).

A further sub-sample (*ca.* 1 cm³) was taken from well-cemented intervals and cast into 25-mm diameter epoxy mount (Mt. Simon sampled at 1680.4 m/5513.2 ft (see Fig. 2c-d), Eau Claire at 1096.5 m/3597.5 ft). As is standard practice at WiscSIMS, several grains of microanalytical reference materials (RMs) were embedded in the center of each mount for the purposes of monitoring instrumental drift and for correcting sample matrix effects during subsequent isotope ratio analyses by SIMS. The following RMs were used: dolomite “UW6220” ($\delta^{18}\text{O}=22.60\text{\textperthousand}$ relative to Vienna Mean Standard Ocean Water (VSMOW), $\delta^{13}\text{C}=0.84\text{\textperthousand}$ relative to the Vienna PeeDee Belemnite standard (VPDB); Śliwiński et al., 2016a,b) and quartz “UWQ-1” ($\delta^{18}\text{O}=12.33\text{\textperthousand}$ VSMOW; Kelly et al., 2007). The mount was then polished to a 0.25- μm finish, cleaned with ethanol and deionized water, and lastly coated with a thin layer of gold (25 nm thickness) to make the sample surface electrically conductive for subsequent $\delta^{13}\text{C}$ and $\delta^{18}\text{O}$ analyses by SIMS. The gold coat was later removed and replaced with a coat of carbon (25 nm thickness) for electron probe microanalysis (EPMA) to

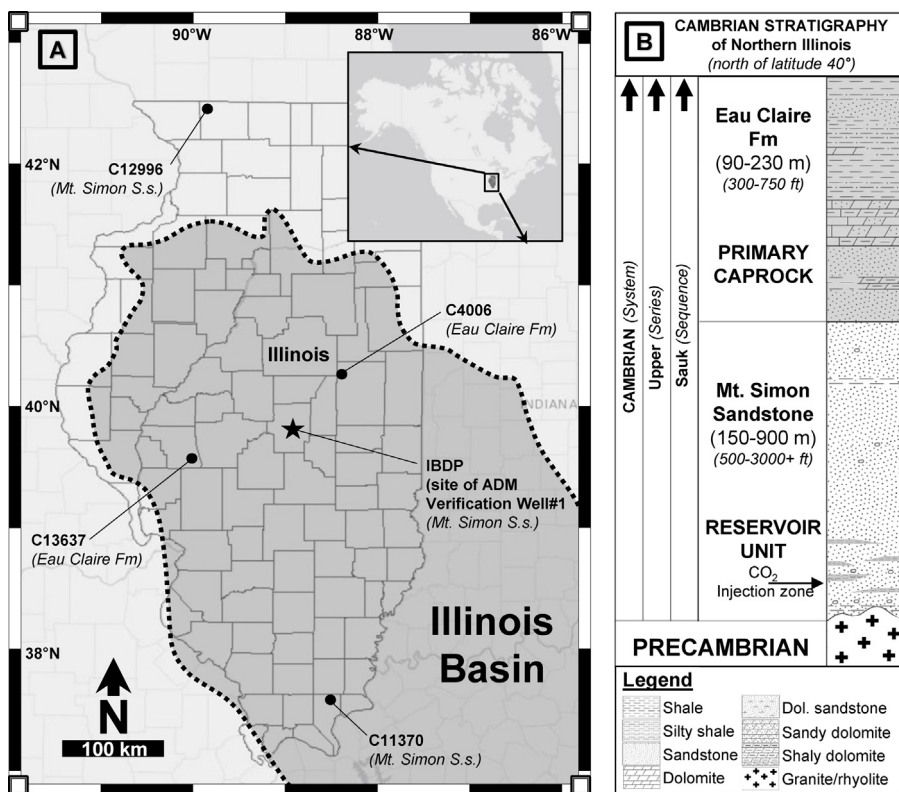


Fig. 1. (A) Locations of drill holes sampled for this study of the upper Mt. Simon Sandstone and the overlying Eau Claire shale. These units respectively comprise the reservoir and the caprock (impermeable seal) at the Illinois Basin Decatur Project (IBDP), a demonstration site for the feasibility of engineered CO₂ storage in a deep saline aquifer. Geographic extent of Illinois Basin traced after Kolata and Nimz (2010). (B) Cambrian stratigraphy of the Illinois Basin (north of latitude 40°N); only the portion that is relevant to this study is shown. Modified after Kolata (2005).

determine the chemical composition of different carbonate cement zones.

Samples were examined petrographically by means of high-resolution back-scattered electron (BSE) and cathodoluminescence (CL, Gatan PanaCL) SEM imaging; in the case of the Mt. Simon Sandstone sample, CL-imaging of quartz cements (quartz-overgrowths) was essential to establishing the relative order of major stages in the quartz and carbonate cementation histories (SA 1). CL-imaging of quartz cements was performed with the sample very thinly coated with carbon (~5 nm) to maximize the signal strength; no filters were employed. We found that many of the CL-features visible in the images of quartz cements that follow were either heavily subdued or not discernable altogether with a standard thickness carbon coat (25 nm).

We provide here an abridged account of the SIMS and EPMA methodologies. The interested reader is referred to Śliwiński et al. (2016a,b,c) for further details. *In situ* carbon and oxygen isotope ratio measurements were performed using a CAMECA IMS 1280 large radius multicollector ion microprobe (Department of Geoscience, University of Wisconsin-Madison). Measured isotope ratios are reported using conventional δ -notation, which expresses the per mil (‰) deviation of a measured ratio from the value of an internationally accepted reference material (VSMOW for $\delta^{18}\text{O}$ and VPDB for $\delta^{13}\text{C}$ analyses).

The analytical precision of SIMS $\delta^{18}\text{O}$ measurements at Wisc-SIMS is typically $\pm 0.3\%$ (2SD, standard deviations) for a sample spot-size of 10 micrometers and $\pm 0.7\%$ (2SD) for 3-micrometer spots; this follows from the spot-to-spot repeatability of replicate measurements ($n=8$) of a running standard (or drift monitoring material, in this case dolomite "UW6220") which bracket each set of about 10 sample analyses. For $\delta^{13}\text{C}$ measurements employing a 6- μm spot-size, the typical precision is 0.6–1.2% (2SD).

The analytical accuracy of SIMS $\delta^{18}\text{O}$ and $\delta^{13}\text{C}$ measurements is affected by instrumental mass fractionation and sample matrix effects (collectively referred to as the 'bias'; e.g., Eiler et al., 1997; Hervig et al., 1992; Kita et al., 2009; Valley and Kita, 2009). This bias is a measure of the per mil (‰) difference between measured 'raw' and 'true' (i.e., VPDB or VSMOW) values of $\delta^{13}\text{C}$ or $\delta^{18}\text{O}$. For a given configuration of the secondary ion mass spectrometer, the influence of instrumental parameters to total bias during an analytical session can be held nearly constant; any instrumental drift that occurs can be monitored and corrected by regularly analyzing a running standard (or drift-monitoring material). For minerals that exhibit solid-solution behavior, this leaves the component of total bias that is a function of variable chemical composition (i.e., the sample matrix effect) in need of calibrating. The development of reference materials along with calibration schemes for the analysis of carbonate mineral compositions that fall along the dolomite-ankerite solid solution series was previously reported by Śliwiński et al. (2016a,b). These bias corrections require that the chemical composition in the immediate vicinity of each SIMS pit be known with a high degree of precision, especially in the case of low-Fe dolomites (up to several wt.% Fe). To correct the data presented here, chemical analyses were performed by EPMA (using a CAMECA SX-51 at the Cameron Electron Microprobe Laboratory, Department of Geoscience, University of Wisconsin-Madison).

The accuracy of sample analyses is determined in large part by the residuals of the SIMS $\delta^{18}\text{O}$ and $\delta^{13}\text{C}$ calibration curves for carbonates of dolomite-ankerite series. The residuals reflect how well the bias correction scheme for each isotope system reproduces data for a suite of 13 reference materials in relation to the certified reference material NBS-19. For O-isotope analyses employing a 10- μm diameter spot-size and C-isotope analyses employing a 6- μm spot-size, the residual is typically constrained to $\pm 0.3\%$ (2SD).

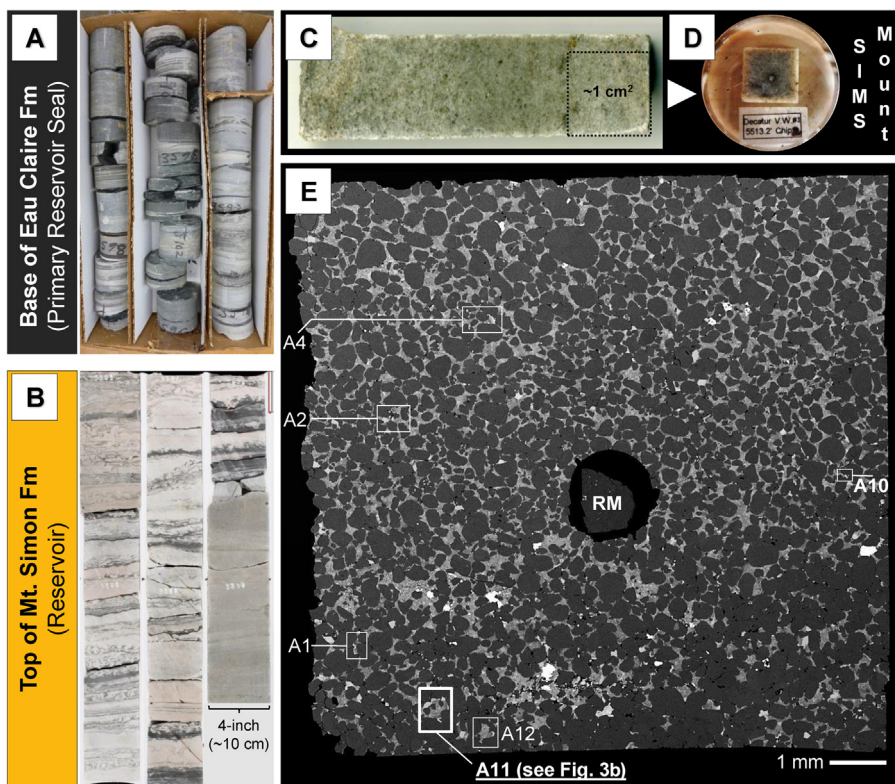


Fig. 2. From core to *in situ* isotope microanalysis of mineral cements. Segments of core showing (A) the silty-shaly Eau Claire Formation, the primary caprock (seal) (well C13637, depth interval: 1095–1097 m/3592–3598.5 ft) and (B) the upper Mt. Simon sandstone reservoir at the Illinois Basin Decatur Project site (ADM Verification Well #1, depth interval: 1678–1679.5 m/5505–5510 ft; see Fig. 1). (Image in (B) modified after Fig. 4.1 in Palkovic, 2015). Sample preparation at WiscSIMS involves casting a small subsample of core (~1 cm³) from C) into a 1-in. (25-mm) diameter epoxy mount (D) and co-mounting an appropriate reference material (RM) in the center. Areas of interest for analysis (e.g., 'A11' in E; see also SA 1) are identified by BSE-SEM-imaging (the quartz-grain framework of this sample is uniformly dark gray in this image, whereas the light-gray shades represent pore-filling, chemically zoned dolomite-ankerite cements. Pyrite and K-feldspar appear white).

The residual increases slightly to $\pm 0.4\text{‰}$ (2SD) when analyzing O-isotope ratios using a 3-μm diameter spot-size Śliwiński et al. (2016a,b).

3. Results

3.1. Chemical zoning patterns in carbonate cements

On the basis of BSE imaging by SEM – a mode that is sensitive to variations in chemical composition – we identified six major stages of carbonate (dolomite-ankerite) cementation within the examined sandstone bed of the upper Mt. Simon Fm. Each successive stage appears as a concentric zone with a distinct 'BSE texture' and sharp compositional boundaries with the preceding and/or succeeding cement zones (Fig. 3b; SA 1). Texturally, zones 4–6 are predominately characterized by layering/banding; this is evidenced by subtle, concentric, within-zone variations in the shades of gray seen in BSE images (indicative of changes in chemical composition that are more subtle within zones than they are among zones). In contrast, the texture of zones 1–3 can be described as 'mottled' and suggests some degree of recrystallization (*sensu* Machel, 1997). The carbonate cement morphology takes the form of poikilotopic crystals measuring up to ~500 μm across, with well-developed crystal faces where pore space permits (Fig. 3b, SA 1).

Carbonate cement zones were classified in terms of chemical composition/mineralogy according to the scheme of Chang et al. (1998), where the dolomite-ankerite solid-solution series is subdivided on the basis of Fe-content as follows: (1) non-ferroan dolomite (NFD; Fe#: 0.0–0.1, where Fe#=molar Fe/(Mg + Fe), equivalent to 0–5 mol% Fe (*i.e.* Fe/(Ca + Mg + Fe))), (2) ferroan

dolomite (FD; Fe#: 0.1–0.2, equivalent to 5–10 mol% Fe), and (3) ankerite (Ank; Fe#>0.2, equivalent to >10 mol% Fe). Accordingly, zones 1 and 2 straddle the boundary between ferroan dolomite and ankerite; zone 3 is a low-Fe ankerite (Fe#: 0.20–0.25); zone 4 is a ferroan dolomite; and zones 5 and 6 are distinctly Fe-rich ankerites (Fe#'s extending to 0.5; Fig. 4a–b, Table 1).

Six major stages of carbonate (dolomite-ankerite) cementation were also identified within the examined Eau Claire shale sample (Figs. 3a, 5), although we cannot establish how these correlate to the cement zones in the Mt. Simon Sandstone. The cement morphology is dominated by euhedral crystals, typically measuring <100 μm across. The chemical zoning pattern is concentric, with no major dissolution features or mottled textures that would suggest some degree of recrystallization (Figs. 3a, 5). An abrupt change in composition is noted between: zones 0 (NFD) and 1a (FD-Ank); zones 1b (FD) and 2a (Ank); and again between zones 2b (Ank) and 3 (NFD) (Figs. 5 and 6a–b). In contrast, the change in composition is more gradational between zones 1a (Ank-FD) and 1b (FD) and again between zones 2a and 2b; nonetheless, two distinct sub-domains are evident in both instances in BSE-imagery: a relatively Fe-rich inner domain (zones 1a and 2a) and a less Fe-rich outer domain (zones 1b and 2b; Figs. 5 and 6a–b).

3.2. Trends in the isotopic composition ($\delta^{13}\text{C}$ and $\delta^{18}\text{O}$) of carbonate cements

The results of *in situ* SIMS $\delta^{13}\text{C}$ and $\delta^{18}\text{O}$ analyses are summarized in Tables 1–3 and are presented graphically in Figs. 3–7. Throughout this article, values of $\delta^{13}\text{C}$ are expressed relative to the VPDB reference value, whereas those of $\delta^{18}\text{O}$ are expressed rela-

Table 1

Isotopic composition ($\delta^{13}\text{C}$ and $\delta^{18}\text{O}$ by SIMS) and major element chemistry (by EPMA) of carbonate cements in the upper Mt. Simon Sandstone (ADM Verification Well #1, depth = 1680.4 m/5513.2 ft). Refer to SA 1 for petrographic context of each spot-analysis.

Session specific sample I.D.	SIMS session	Sample region	Spot-size (μm)	$\delta^{18}\text{O}\%$ VPDB	$\delta^{18}\text{O}\%$ VSMOW	2SD	Session specific sample I.D.	$\delta^{13}\text{C}\%$ VPDB	2SD	Zone	Fe#	% MgCO_3 (mol.%)	% CaCO_3 (mol.%)	% FeCO_3 (mol.%)	% MnCO_3 (mol.%)
20140513@598.asc	S7	Area 11	10	-8.4	22.3	0.4	20140404@268.asc	-3.2	1.1	1	0.231	39.04	48.14	11.75	1.08
20140513@595.asc	S7	Area 11	10	-12.3	18.2	0.4	20140404@269.asc	-2.8	1.1	1	0.238	35.37	50.59	11.07	2.97
20140513@599.asc	S7	Area 11	10	-9.9	20.7	0.4	20140404@269.asc	-2.8	1.1	1	0.238	35.37	50.59	11.07	2.97
20140513@597.asc	S7	Area 11	10	-8.9	21.8	0.4	20140404@267.asc	-1.5	1.1	1	0.228	38.53	49.42	11.40	0.66
20140513@596.asc	S7	Area 11	10	-9.1	21.5	0.4	20140404@270.asc	-1.5	1.1	1	0.208	39.20	49.95	10.27	0.59
20140513@607.asc	S7	Area 11	10	-10.2	20.3	0.3	20140404@271.asc	-0.4	1.1	2	0.197	39.57	50.18	9.70	0.55
20140513@606.asc	S7	Area 11	10	-10.3	20.3	0.3	20140404@272.asc	-0.5	1.1	2	0.200	40.90	48.35	10.23	0.53
20140513@605.asc	S7	Area 11	10	-12.7	17.8	0.3	20140404@273.asc	-3.4	1.1	3	0.208	38.08	49.52	10.02	2.37
20140513@604.asc	S7	Area 11	10	-9.1	21.6	0.3	20140404@274.asc	-0.3	1.1	4	0.160	42.72	48.32	8.16	0.80
20140513@586.asc	S7	Area 11	10	-9.5	21.1	0.2	20140404@279.asc	0.2	1.2	4	0.193	39.05	49.75	9.32	1.88
20140513@585.asc	S7	Area 11	10	-9.9	20.7	0.2	20140404@279.asc	0.2	1.2	4	0.193	39.05	49.75	9.32	1.88
20140513@591.asc	S7	Area 11	10	-8.2	22.5	0.4	20140404@286.asc	-0.4	1.2	4	0.141	41.97	50.71	6.88	0.44
20140513@592.asc	S7	Area 11	10	-7.6	23.1	0.4	20140404@283.asc	-1.3	1.2	4	0.120	42.22	51.37	5.74	0.67
20140513@592.asc	S7	Area 11	10	-7.6	23.1	0.4	20140404@282.asc	-1.2	1.2	4	0.162	39.67	51.32	7.58	1.42
20140513@584.asc	S7	Area 11	10	-13.7	16.8	0.2	20140404@281.asc	-2.4	1.2	5	0.213	35.81	51.95	9.69	2.56
20140513@583.asc	S7	Area 11	10	-10.2	20.4	0.2	20140404@280.asc	-6.2	1.2	6	0.338	28.33	54.78	14.48	2.41
20140513@581.asc	S7	Area 11	10	-12.2	18.3	0.2	20140404@285.asc	-6.2	1.2	6	0.390	24.87	56.19	15.95	2.98
20140513@594.asc	S7	Area 11	10	-12.7	17.8	0.4	20140404@285.asc	-6.2	1.2	6	0.390	24.87	56.19	15.95	2.98
20140513@582.asc	S7	Area 11	10	-13.5	17.0	0.2	20140404@284.asc	-7.1	1.2	6	0.483	20.93	55.43	19.50	4.14
20140513@593.asc	S7	Area 11	10	-13.8	16.7	0.4	20140404@284.asc	-7.1	1.2	6	0.483	20.93	55.43	19.50	4.14
20140107@158.asc	S2	Area 4	10	-10.9	19.7	0.5	20140404@243.asc	-1.0	0.6	2	0.182	39.07	51.75	8.71	0.47
20140107@155.asc	S2	Area 4	10	-11.0	19.6	0.5	20140404@244.asc	-1.5	0.6	4	0.184	39.41	50.79	8.90	0.90
20140107@156.asc	S2	Area 4	10	-10.4	20.2	0.5	20140404@245.asc	-0.9	0.6	4	0.156	39.95	52.03	7.38	0.64
20140107@157.asc	S2	Area 4	10	-14.1	16.4	0.5	20140404@246.asc	-5.4	0.6	5	0.251	34.37	50.83	11.54	3.27
20140107@164.asc	S2	Area 4	10	-8.5	22.1	0.3	20140404@249.asc	-5.7	0.6	6?	0.294	32.24	53.33	13.40	1.02
20140107@163.asc	S2	Area 4	10	-13.2	17.3	0.3	20140404@247.asc	-7.3	0.6	6	0.430	22.49	57.42	16.73	3.36
20140107@165.asc	S2	Area 4	10	-13.5	17.0	0.3	20140404@248.asc	-8.3	0.6	6	0.412	23.51	57.14	16.32	3.04
20140224@367.asc	S4	Area 2	3	-13.4	17.1	1.0	20140404@256.asc	-8.6	1.1	6	0.413	24.16	55.98	16.97	2.89
20140224@368.asc	S4	Area 2	3	-11.7	18.8	1.0	20140404@257.asc	-6.5	1.1	6	0.376	26.47	55.41	15.95	2.17
20140107@144.asc	S2	Area 2	10	-11.9	18.7	0.5	20140404@257.asc	-6.5	1.1	6	0.376	26.47	55.41	15.95	2.17
20140107@145.asc	S2	Area 2	10	-12.2	18.4	0.5	20140404@257.asc	-6.5	1.1	6	0.376	26.47	55.41	15.95	2.17
20140224@371.asc	S4	Area 2	3	-14.1	16.4	1.0	20140404@256.asc	-8.6	1.1	6	0.413	24.16	55.98	16.97	2.89
20140107@143.asc	S2	Area 2	10	-14.2	16.3	0.5	20140404@259.asc	-5.9	1.1	5	0.260	34.84	49.53	12.23	3.41
20140107@142.asc	S2	Area 2	10	-14.4	16.0	0.5	20140404@259.asc	-5.9	1.1	5	0.260	34.84	49.53	12.23	3.41
20140107@141.asc	S2	Area 2	10	-10.2	20.4	0.5	20140404@258.asc	-0.8	1.1	4	0.163	41.17	50.27	7.98	0.58
20140107@141.asc	S2	Area 2	10	-10.2	20.4	0.5	20140404@260.asc	-1.9	1.1	4	0.163	41.17	50.27	7.98	0.58
20140107@140.asc	S2	Area 2	10	-11.0	19.6	0.5	20140404@261.asc	-2.6	1.1	4	0.197	39.10	50.62	9.63	0.65
20140107@139.asc	S2	Area 2	10	-10.5	20.1	0.5	-	-	-	3	0.239	33.73	51.53	10.59	4.15
20140224@348.asc	S4	Area 10	3	-6.2	24.6	0.6	20140404@231.asc	0.9	0.7	4	0.125	41.55	51.93	5.86	0.66
20140224@338.asc	S4	Area 10	3	-5.5	25.2	0.9	20140404@231.asc	0.9	0.7	4	0.125	41.55	51.93	5.86	0.66
20140224@347.asc	S4	Area 10	3	-6.8	23.9	0.6	20140404@231.asc	0.9	0.7	4	0.125	41.55	51.93	5.86	0.66
20140107@175.asc	S2	Area 10	10	-6.9	23.8	0.2	20140404@232.asc	0.6	0.7	4	0.125	41.55	51.93	5.86	0.66
20140107@177.asc	S2	Area 10	10	-6.9	23.8	0.2	20140404@238.asc	0.7	0.7	4	0.125	41.55	51.93	5.86	0.66
20140107@177.asc	S2	Area 10	10	-6.9	23.8	0.2	20140404@233.asc	-0.4	0.7	4	0.125	41.55	51.93	5.86	0.66
20140224@339.asc	S4	Area 10	3	-8.5	22.2	0.9	20140404@235.asc	-4.8	0.7	6	0.352	28.59	53.98	15.49	1.94

20140107@176.asc	S2	Area 10	10	-12.2	18.3	0.2	20140404@235.asc	-4.8	0.7	6	0.352	28.59	53.98	15.49	1.94
20140107@178.asc	S2	Area 10	10	-12.5	18.0	0.2	20140404@235.asc	-4.8	0.7	6	0.352	28.59	53.98	15.49	1.94
20140224@335.asc	S4	Area 10	3	-9.9	20.7	0.9	20140404@234.asc	-7.2	0.7	6	0.401	24.98	55.46	16.66	2.90
20140224@336.asc	S4	Area 10	3	-11.2	19.4	0.9	20140404@234.asc	-7.2	0.7	6	0.401	24.98	55.46	16.66	2.90
20140224@349.asc	S4	Area 10	3	-12.2	18.3	0.6	20140404@234.asc	-7.2	0.7	6	0.401	24.98	55.46	16.66	2.90
20140224@337.asc	S4	Area 10	3	-12.3	18.3	0.9	20140404@234.asc	-7.2	0.7	6	0.401	24.98	55.46	16.66	2.90
20140224@340.asc	S4	Area 10	3	-13.1	17.4	0.9	20140404@237.asc	-7.7	0.7	6	0.406	24.71	55.48	16.83	2.97
20140224@345.asc	S4	Area 10	3	-13.6	16.9	0.6	20140404@237.asc	-7.7	0.7	6	0.406	24.71	55.48	16.83	2.97
20140224@346.asc	S4	Area 10	3	-13.6	16.9	0.6	20140404@236.asc	-7.9	0.7	6	0.287	41.04	55.28	14.99	2.30
20140107@199.asc	S2	Area 1	10	-10.1	20.5	0.5	-	-	-	4	0.161	40.83	50.71	7.83	0.63
20140107@200.asc	S2	Area 1	10	-11.2	19.4	0.5	-	-	-	3?	0.221	35.82	52.46	10.14	1.58
20140107@198.asc	S2	Area 1	10	-13.8	16.6	0.5	-	-	-	5	0.228	34.69	52.30	10.18	2.83
20140107@197.asc	S2	Area 1	10	-12.1	18.4	0.5	-	-	-	6	0.364	26.01	56.82	14.85	2.33
20140107@196.asc	S2	Area 1	10	-14.1	16.4	0.5	-	-	-	6	0.422	23.06	56.69	16.78	3.46
20140107@195.asc	S2	Area 1	10	-12.8	17.7	0.5	-	-	-	6	0.394	24.50	56.84	15.78	2.88
20140107@190.asc	S2	Area 1	10	-10.8	19.7	0.5	-	-	-	2	0.228	35.48	51.91	10.43	2.18
20140107@191.asc	S2	Area 1	10	-11.1	19.4	0.5	-	-	-	2	0.228	35.48	51.91	10.43	2.18
20140107@192.asc	S2	Area 1	10	-9.4	21.2	0.5	-	-	-	4	0.169	39.75	51.40	8.11	0.74
20140107@193.asc	S2	Area 1	10	-12.3	18.2	0.5	-	-	-	5	0.364	25.91	57.13	14.80	2.16
20140107@194.asc	S2	Area 1	10	-11.4	19.1	0.5	-	-	-	5	0.319	29.09	54.66	13.53	2.72
-	-	Area 12	-	-	-	-	20140405@415.asc	-0.9	1.0	1	0.196	37.37	51.88	9.02	1.73
-	-	Area 12	-	-	-	-	20140405@416.asc	-2.0	1.0	1	0.236	35.64	51.20	11.02	2.15
-	-	Area 12	-	-	-	-	20140405@417.asc	-1.6	1.0	1	0.242	37.21	50.30	11.82	0.66
-	-	Area 12	-	-	-	-	20140405@418.asc	-1.3	1.0	1	0.198	39.68	49.92	9.79	0.61
-	-	Area 12	-	-	-	-	20140405@419.asc	-1.6	1.0	1	0.252	36.21	49.38	12.19	2.22
-	-	Area 12	-	-	-	-	20140405@420.asc	-3.0	1.0	1	0.174	39.52	51.61	8.31	0.56
-	-	Area 12	-	-	-	-	20140405@421.asc	-0.7	1.0	1	0.209	38.96	50.02	10.31	0.71
-	-	Area 12	-	-	-	-	20140405@422.asc	-0.8	1.0	1	0.174	39.52	51.61	8.31	0.56
-	-	Area 12	-	-	-	-	20140405@427.asc	-8.1	0.8	6	0.427	23.77	55.57	17.64	3.03
-	-	Area 12	-	-	-	-	20140405@428.asc	-5.8	0.8	6	0.348	28.53	54.37	15.25	1.85
-	-	Area 12	-	-	-	-	20140405@429.asc	-4.7	0.8	5	0.236	35.48	50.59	10.96	2.97
-	-	Area 12	-	-	-	-	20140405@430.asc	0.5	0.8	4	0.168	40.34	50.95	8.14	0.58
-	-	Area 12	-	-	-	-	20140405@431.asc	-0.5	0.8	4	0.129	43.74	49.17	6.48	0.62
-	-	Area 12	-	-	-	-	20140405@432.asc	-0.4	0.8	2	0.210	38.07	51.17	10.13	0.62
-	-	Area 12	-	-	-	-	20140405@433.asc	-0.1	0.8	2	0.178	40.76	49.92	8.86	0.46
-	-	Area 12	-	-	-	-	20140405@434.asc	-2.3	0.8	1	0.257	35.14	50.59	12.12	2.15

Table 2

Isotopic composition ($\delta^{13}\text{C}$ and $\delta^{18}\text{O}$ by SIMS) and major element chemistry (by EPMA) of carbonate cements in the Eau Claire shale (C13637, depth = 1096.5 m/3597.5 ft). Refer to SA 1 for petrographic context of each spot-analysis.

Session specific sample I.D.	SIMS session	Sample region	Spot-size (μm)	$\delta^{18}\text{O}_{\text{VPDB}}$ ‰	$\delta^{18}\text{O}_{\text{VSMOW}}$ ‰	2SD	$\delta^{13}\text{C}_{\text{VPDB}}$ ‰	2SD	Zone	Fe#	%MgCO ₃ (mol.%)	%CaCO ₃ (mol.%)	%FeCO ₃ (mol.%)	%MnCO ₃ (mol.%)
20140212@156.asc	S3	A1 R1	10	-4.2	26.6	0.2	—	—	Z0	0.007	41.91	57.74	0.31	0.04
20140212@163.asc	S3	A2 R2	10	-4.4	26.3	0.2	—	—	Z0	0.007	41.91	57.74	0.31	0.04
20140212@171.asc	S3	A3 R3	10	-5.3	25.5	0.2	—	—	Z0	0.007	41.91	57.74	0.31	0.04
20140212@178.asc	S3	A4 R4a	10	-5.2	25.6	0.2	—	—	Z0	0.007	41.91	57.74	0.31	0.04
20140212@206.asc	S3	A6 R6	10	-4.6	26.1	0.4	—	—	Z0	0.007	41.91	57.74	0.31	0.04
20140405@443.asc	S5	An-1	6	—	—	—	4.2	0.8	Z0	0.007	41.65	58.00	0.31	0.04
20140405@444.asc	S5	An-1	6	—	—	—	3.1	0.8	Z0	0.007	41.65	58.00	0.31	0.04
20140405@455.asc	S5	An-2	6	—	—	—	2.6	0.7	Z0	0.007	41.65	58.00	0.31	0.04
20140405@491.asc	S5	A3	6	—	—	—	3.9	0.8	Z0	0.007	41.65	58.00	0.31	0.04
Zone 0 average	—	—	—	-4.7	26.0	—	3.5	—	—	0.007	41.79	57.86	0.31	0.04
2SD	—	—	—	0.9	1.0	—	1.5	—	—	0.000	0.27	0.27	0.00	0.00
20140212@164.asc	S3	A2 R2	10	-5.9	24.9	0.2	—	—	Z1a	0.225	31.40	58.90	9.10	0.50
20140212@166.asc	S3	A2 R2	10	-6.2	24.5	0.2	—	—	Z1a	0.225	31.40	58.90	9.10	0.50
20140405@447.asc	S5	An-1	6	—	—	—	9.3	0.8	Z1a	0.218	31.13	59.65	8.69	0.53
20140405@448.asc	S5	An-1	6	—	—	—	9.7	0.8	Z1a	0.196	33.54	57.81	8.19	0.46
20140405@456.asc	S5	An-2	6	—	—	—	8.7	0.7	Z1a	0.168	36.00	56.33	7.26	0.41
20140405@462.asc	S5	An-3	6	—	—	—	9.6	0.7	Z1a	0.236	31.35	58.38	9.66	0.61
20140405@471.asc	S5	A5 exp	6	—	—	—	11.3	0.7	Z1a	0.236	31.35	58.38	9.66	0.61
20140405@472.asc	S5	A5 exp	6	—	—	—	12.5	0.7	Z1a	0.236	31.35	58.38	9.66	0.61
20140405@492.asc	S5	A3	6	—	—	—	7.4	0.8	Z1a	0.182	34.73	57.10	7.75	0.42
20140405@508.asc	S5	A5 exp1	6	—	—	—	8.1	0.9	Z1a	0.217	31.44	59.33	8.75	0.48
Zone 1a average	—	—	—	-6.0	24.7	—	9.6	—	—	0.214	32.37	58.32	8.78	0.51
2SD	—	—	—	0.5	0.5	—	3.3	—	—	0.048	3.50	2.02	1.67	0.15
20140212@172.asc	S3	A3 R3	10	-5.4	25.4	0.2	—	—	Z1b	0.167	34.46	57.77	6.89	0.88
20140212@179.asc	S3	A4 R4a	10	-5.0	25.8	0.2	—	—	Z1b	0.099	37.18	58.32	4.09	0.41
20140212@180.asc	S3	A4 R4a	10	-5.6	25.1	0.2	—	—	Z1b	0.120	34.71	59.79	4.72	0.78
20140212@183.asc	S3	A4 R4a	10	-5.7	25.0	0.2	—	—	Z1b	0.121	35.24	59.45	4.88	0.43
20140212@198.asc	S3	A4 R4b	10	-5.7	25.1	0.4	—	—	Z1b	0.127	35.47	58.90	5.15	0.49
20140212@461.asc	S3	A1 R1	10	-5.9	24.9	0.2	—	—	Z1b	0.092	38.65	57.02	3.90	0.43
20140212@471.asc	S3	A5 SR1	10	-5.6	25.2	0.2	—	—	Z1b	0.114	36.27	58.63	4.68	0.42
20140405@467.asc	S5	An-3	6	—	—	—	10.4	0.7	Z1b	0.127	35.05	59.38	5.10	0.47
20140405@468.asc	S5	An-3	6	—	—	—	11.6	0.7	Z1b	0.127	35.05	59.38	5.10	0.47
20140405@482.asc	S5	A5 exp	6	—	—	—	13.1	0.8	Z1b	0.123	36.55	57.95	5.13	0.36
20140405@486.asc	S5	A5 exp	6	—	—	—	14.3	0.8	Z1b	0.123	36.55	57.95	5.13	0.36
20140405@493.asc	S5	A3	6	—	—	—	7.3	0.8	Z1b	0.137	35.06	58.92	5.56	0.46
20140405@516.asc	S5	A5 exp5	6	—	—	—	11.7	0.9	Z1b	0.107	38.10	56.84	4.58	0.49
20140405@517.asc	S5	A5 exp6	6	—	—	—	9.4	0.9	Z1b	0.132	35.46	58.48	5.42	0.64
20140405@518.asc	S5	A5 exp7	6	—	—	—	7.2	0.9	Z1b	0.141	35.97	57.10	5.90	1.03
Zone 1b average	—	—	—	-5.5	25.2	—	10.6	—	—	0.124	35.98	58.39	5.08	0.54
2SD	—	—	—	0.6	0.6	—	5.2	—	—	0.036	2.47	1.88	1.44	0.40
20140212@173.asc	S3	A3 R3	10	-8.0	22.6	0.2	—	—	Z2a	0.289	27.41	61.10	11.14	0.35
20140212@181.asc	S3	A4 R4a	10	-7.5	23.2	0.2	—	—	Z2a	0.253	30.93	59.08	9.52	0.47
20140405@445.asc	S5	An-1	6	—	—	—	6.6	0.8	Z2a	0.295	29.20	58.21	12.26	0.33
20140405@461.asc	S5	An-3	6	—	—	—	5.9	0.7	Z2a	0.231	32.05	57.84	9.62	0.50
20140405@469.asc	S5	An-3	6	—	—	—	7.2	0.7	Z2a	0.299	28.74	58.51	12.26	0.50
20140405@509.asc	S5	A5 exp2	6	—	—	—	7.8	0.9	Z2a	0.290	29.78	57.62	12.18	0.42
20140405@519.asc	S5	A5 exp2	6	—	—	—	9.7	0.9	Z2a	0.272	28.73	60.24	10.73	0.31
Zone 2a average	—	—	—	-7.7	22.9	—	7.4	—	—	0.276	29.55	58.94	11.10	0.41

2SD	–	–	–	0.8	0.8	–	2.9	–	–	0.050	3.08	2.59	2.41	0.16
20140212@158.asc	S3	A1 R1	10	-8.2	22.4	0.2	–	–	Z2b	0.245	31.11	58.47	10.12	0.31
20140212@174.asc	S3	A3 R3	10	-8.0	22.6	0.2	–	–	Z2b	0.245	31.79	57.48	10.32	0.41
20140212@182.asc	S3	A4 R4a	10	-8.2	22.4	0.2	–	–	Z2b	0.238	32.13	57.38	10.05	0.44
20140212@184.asc	S3	A4 R4a	10	-8.0	22.7	0.2	–	–	Z2b	0.232	29.94	60.58	9.03	0.45
20140212@210.asc	S3	A6 R6	10	-7.2	23.4	0.4	–	–	Z2b	0.270	30.56	57.62	11.30	0.52
20140212@216.asc	S3	A5 R5	10	-8.5	22.2	0.4	–	–	Z2b	0.237	31.20	58.67	9.70	0.43
20140212@462.asc	S3	A1 R1	10	-8.9	21.7	0.2	–	–	Z2b	0.253	32.66	55.73	11.00	0.60
20140212@473.asc	S3	A5 SR1	10	-7.8	22.8	0.2	–	–	Z2b	0.232	33.21	56.51	10.04	0.24
20140212@479.asc	S3	A5 SR1	10	-8.1	22.6	0.3	–	–	Z2b	0.229	32.44	57.34	9.64	0.58
20140405@446.asc	S5	An-1	6	–	–	–	7.1	0.8	Z2b	0.222	34.05	55.94	9.69	0.32
20140405@473.asc	S5	A5 exp	6	–	–	–	9.2	0.7	Z2b	0.243	32.82	56.26	10.53	0.39
20140405@483.asc	S5	A5 exp	6	–	–	–	10.2	0.8	Z2b	0.238	32.62	56.69	10.17	0.52
20140405@484.asc	S5	A5 exp	6	–	–	–	10.8	0.8	Z2b	0.286	30.98	56.13	12.42	0.47
Zone 2b average	–	–	–	-8.1	22.5	–	9.3	–	–	0.244	31.96	57.29	10.31	0.44
2SD	–	–	–	0.9	0.9	–	3.3	–	–	0.035	2.32	2.70	1.73	0.21
20140212@175.asc	S3	A3 R3	10	-7.6	23.1	0.2	–	–	Z3	0.094	40.12	55.55	4.17	0.15
20140212@191.asc	S3	A4 R4a	10	-7.6	23.1	0.4	–	–	Z3	0.109	38.69	56.38	4.74	0.19
20140212@193.asc	S3	A4 R4b	10	-8.2	22.5	0.4	–	–	Z3	0.089	39.90	56.00	3.90	0.20
20140212@195.asc	S3	A4 R4b	10	-6.4	24.3	0.4	–	–	Z3	0.081	39.15	57.21	3.42	0.22
20140212@196.asc	S3	A4 R4b	10	-7.9	22.8	0.4	–	–	Z3	0.081	39.15	57.21	3.42	0.22
20140212@197.asc	S3	A4 R4b	10	-6.5	24.2	0.4	–	–	Z3	0.081	39.15	57.21	3.42	0.22
20140212@207.asc	S3	A6 R6	10	-7.0	23.6	0.4	–	–	Z3	0.089	39.90	56.00	3.90	0.20
20140212@209.asc	S3	A6 R6	10	-7.7	23.0	0.4	–	–	Z3	0.096	39.95	55.56	4.27	0.22
20140212@472.asc	S3	A5 SR1	10	-7.8	22.9	0.2	–	–	Z3	0.083	39.53	56.74	3.59	0.15
20140212@478.asc	S3	A5 SR1	10	-6.8	23.8	0.3	–	–	Z3	0.094	42.07	53.39	4.36	0.18
20140212@464.asc	S3	A1 R1	10	-8.8	21.9	0.2	–	–	Z3	0.124	36.92	57.56	5.22	0.29
20140405@449.asc	S5	An-1	6	–	–	–	6.6	0.8	Z3	0.061	40.39	56.78	2.67	0.17
20140405@450.asc	S5	An-1	6	–	–	–	5.5	0.8	Z3	0.050	40.63	57.01	2.14	0.22
20140405@474.asc	S5	A5 exp	6	–	–	–	9.0	0.7	Z3	0.128	38.70	55.35	5.68	0.26
20140405@494.asc	S5	A3	6	–	–	–	5.0	0.8	Z3	0.052	42.61	54.83	2.35	0.20
20140405@495.asc	S5	A3	6	–	–	–	5.8	0.8	Z3	0.052	42.61	54.83	2.35	0.20
20140405@498.asc	S5	An-1	6	–	–	–	7.1	0.8	Z3	0.085	41.60	54.39	3.88	0.14
20140405@515.asc	S5	A5 exp4	6	–	–	–	8.6	0.9	Z3	0.125	38.72	55.52	5.52	0.25
20140405@521.asc	S5	A5 exp10	6	–	–	–	8.3	0.9	Z3	0.106	39.20	55.93	4.66	0.20
20140405@522.asc	S5	A5 exp11	6	–	–	–	7.4	0.9	Z3	0.109	39.01	55.98	4.77	0.23
Zone 3 average	–	–	–	-7.5	23.2	–	7.0	–	–	0.089	39.90	55.97	3.92	0.21
2SD	–	–	–	1.4	1.5	–	2.9	–	–	0.047	2.88	2.17	2.06	0.07

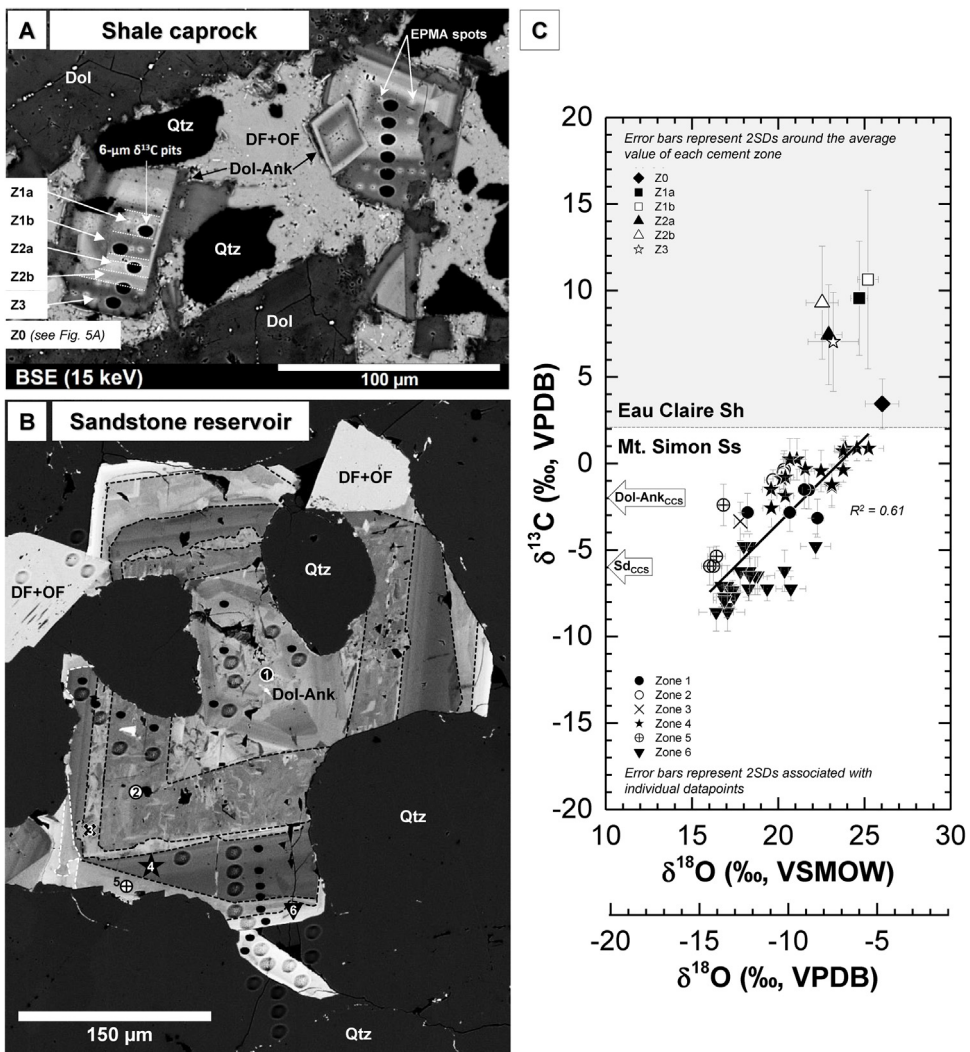


Fig. 3. Preliminary pre-injection characterization by *in situ* isotope microanalysis of the stable carbon and oxygen isotope compositions ($\delta^{13}\text{C}$ and $\delta^{18}\text{O}$, respectively) of individual dolomite-ankerite cement zones in the IBDP reservoir-caprock system (analysis performed by secondary ion mass spectrometry – SIMS; note the analysis pits in A and B). BSE-SEM images showing dolomite-ankerite cements (Dol-Ank) exhibiting micrometer-scale chemo-isotopic zoning in samples of: (A) the Eau Claire shale (Core 13637, depth = 1096.5 m/3597.5 ft; see Fig. 1) and (B) the upper Mt. Simon Sandstone (ADM Verification Well #1, depth = 1680.4 m/5513.2 ft; see Fig. 1), along with corresponding isotopic data (C). Fe-bearing domains appear brighter in these images. Note that due to sampling restrictions, the Eau Claire was sampled from core in a nearby county (~75 km WSW of the IBDP site). Arrows labeled “Dol-Ank” and “Sd” (siderite) in (C) indicate the anticipated $\delta^{13}\text{C}$ values of new carbonates that are expected to form in response to long-term CO_2 storage (see Section 4.1.1 and Table 4). DF + OF = detrital K-feldspar with diagenetic overgrowths; Qtz = Quartz.

tive to VSMOW; for convenience, carbonate $\delta^{18}\text{O}$ values are also tabulated relative to VPDB in Tables 1 and 2. The complete dataset, which includes all measured signals (e.g. count rates, backgrounds, counting statistical errors, etc.) from reference materials and analyzed sample regions, as well as the calibration model parameters used to correct for sample matrix effects, is provided in Supplementary appendices 2–4. Supporting petrographic documentation, which includes individually-annotated SIMS pits, is provided in SA 1. Patches of carbonate cement in multiple sample sub-domains were analyzed to ensure that measured values are representative ('sample regions' in Tables 1–3 and SA 1).

Two distinct data clouds are apparent in cross-plotting $\delta^{13}\text{C}$ vs $\delta^{18}\text{O}$ (Fig. 3c); one is populated by sample data from the upper Mt. Simon sandstone beds, and is generally characterized by progressively more negative $\delta^{13}\text{C}$ values that extend from +1 to −9‰ (VPDB) (to a first-order across cement zones 0 through 3). The other data cloud represents the overlying silty-shaly Eau Claire Fm. and stands in stark contrast, being characterized by positive $\delta^{13}\text{C}$ values that extend from +2 to +16‰ (VPDB) (to a first-order across

zones 0 through 3). Given the small sample subset at this stage of research, however, it is too early to generalize about differences on a formation-wide scale. Please note that based on conventional isotope analyses performed on a larger suite of bulk sample powders, it is known that carbonate $\delta^{13}\text{C}$ variability exists among the four Eau Claire sub-units at the IBDP site (Palkovic, 2015). To a first-order, differences in bulk $\delta^{13}\text{C}$ values – extending from approx. −4‰ to +4‰ VPDB up through the section – correlate to changes in lithology, although depth-dependent changes within individual sub-units are also evident (most clearly seen in the top-most Unit D; refer to Fig. 5.8 in Palkovic, 2015). Additional *in situ* characterizations of lower Eau Claire carbonate cements from across the Illinois Basin are reported elsewhere (Śliwiński et al., 2015, 2016c). What we in-part attempt to demonstrate here is the ability to retrieve another layer of information by interrogating isotopic records on a finer spatial scale. Some potential applications where this may be useful in relation to carbon-sequestration research are discussed later on.

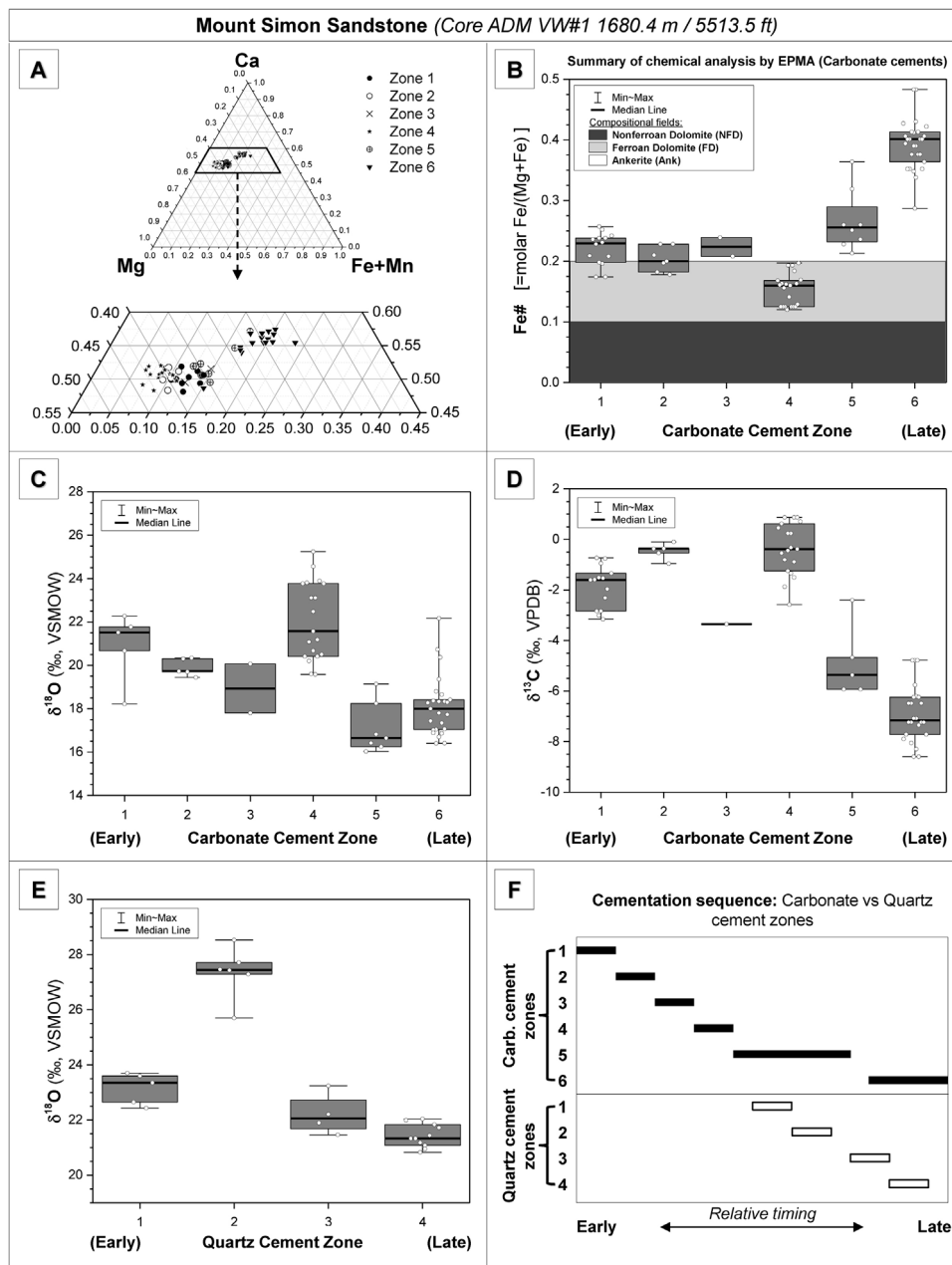


Fig. 4. Select geochemical characteristics of individual carbonate and quartz cement zones within the upper Mt. Simon Sandstone (IBDP, ADM Verification Well #1, depth = 1680.4 m/5513.2 ft). (A) Ca-Mg-Fe ternary diagram showing the cation composition of each major dolomite-ankerite cement zone along with the corresponding (B) Fe/Mg ratios (expressed as the Fe#, or molar Fe/(Mg + Fe)) and stable isotope composition of oxygen ($\delta^{18}\text{O}$; C) and carbon ($\delta^{13}\text{C}$; D). (E) $\delta^{18}\text{O}$ values of individual quartz-overgrowth cement zones. (F) Relative sequence of quartz and carbonate cement zone development. For each cement zone depicted in (B–E), datapoints are offset relative to one another only for clarity.

A moderate linear correlation is apparent in the cross-plot of carbonate $\delta^{13}\text{C}$ and $\delta^{18}\text{O}$ values measured from the Mt. Simon Sandstone (adjusted $R^2 = 0.61$; Fig. 3c). To a first-order, $\delta^{18}\text{O}$ values progressively decrease across early-to-late cement generations from a high of ~22‰ VSMOW (zone 1) to a low of ~16‰ (zone 6) (Figs. 3c and 4c). Notably, however, carbonate $\delta^{18}\text{O}$ values measured from zone 4 abruptly break this trend and transiently increase to a high of ~24‰ (values also increase throughout this stage of cement development from ~20 to 24‰; SA 1). The corresponding carbonate $\delta^{13}\text{C}$ values measured from zones 1 to 3 fall within the relatively narrow range between 0 and -3‰ (VPDB), and then systematically decrease down to -9‰ across zones 4–6 (Fig. 4d; SA 1).

Carbonate $\delta^{13}\text{C}$ and $\delta^{18}\text{O}$ values measured from different cement generations of the Eau Claire shale show no correlation (Fig. 3c). Nonetheless, carbonate $\delta^{18}\text{O}$ values progressively decrease across early-to-late cement generations from a high of ~26‰ (zone 0) to a low of ~23‰ (zone 3) (Fig. 6c). It is notable that, on average, $\delta^{18}\text{O}$ values measured from the shale bed cements are ~4‰ higher than those in the underlying sandstone (same first-order decreasing trend, but with an approx. +4‰ offset; compare Figs. 4c and 6c). The $\delta^{13}\text{C}$ values of the earliest stage of cement development (zone 0) fall between 3 and 4‰ (VPDB) and, in stark contrast to the sandstone beds, increase abruptly during subsequent stages of cement growth; values span the range between +7

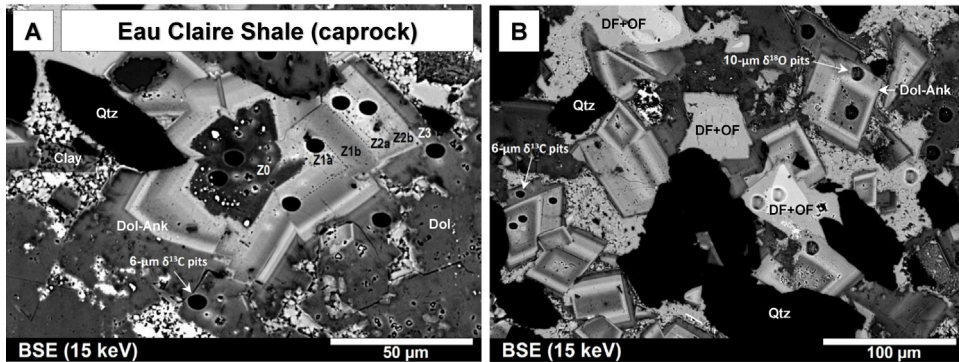


Fig. 5. (A and B) BSE-SEM images showing chemo-isotopically zoned dolomite-ankerite cements (Dol-Ank) in a sample of the Eau Claire shale and representative SIMS isotope microanalysis pits (6- μm $\delta^{13}\text{C}$ and 10- μm $\delta^{18}\text{O}$). Fe-bearing domains appear brighter. (Core 13637, depth = 1096.5 m/3597.5 ft). Z0, Z1a, Z1b, Z2a, Z2b, Z3 = carbonate cement zones. DF + OF = detrital K-feldspar with diagenetic overgrowths; Qtz = Quartz.

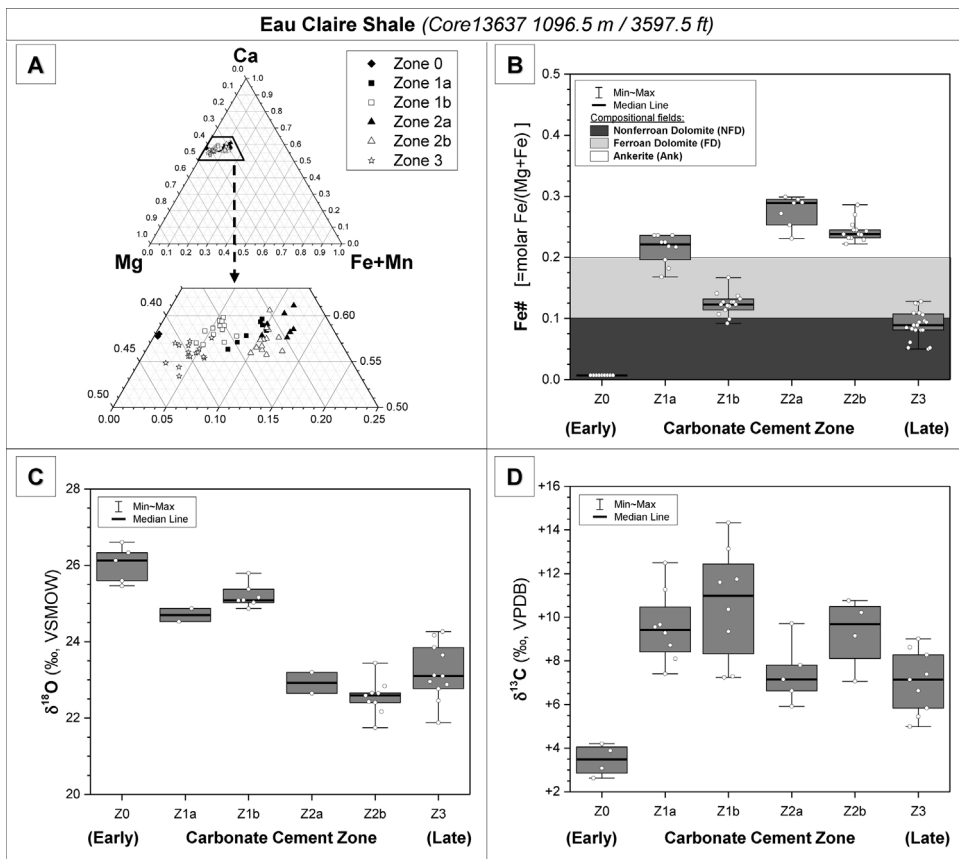


Fig. 6. Select geochemical characteristics of individual carbonate cement zones within the Eau Claire shale (Core 13637, depth = 1096.5 m/3597.5 ft). (A) Ca-Mg-Fe ternary diagram showing the cation composition of each major dolomite-ankerite cement zone along with the corresponding (B) Fe/Mg ratios (expressed as the Fe#, or molar Fe/(Mg+Fe)) and stable isotope composition of oxygen ($\delta^{18}\text{O}$, C) and carbon ($\delta^{13}\text{C}$, D). For each cement zone depicted in (B-D), datapoints are offset relative to one another only for clarity.

and +15‰ across zones 1a and 1b, but fall somewhat to between +6 and +11‰ across zones 2a, 2b, and 3 (Fig. 6d).

3.3. Trends in the isotopic composition ($\delta^{18}\text{O}$) of quartz cement in the upper Mt. Simon Sandstone

On the basis of CL-imaging, we identified four major stages of quartz cementation (QO 1–4) within the examined sandstone bed of the upper Mt. Simon Fm. (Fig. 7; SA 1). Detrital quartz grains are indistinguishable from their respective quartz overgrowths (cement) by BSE-imaging. However, this distinction can be readily made by employing a CL-detector coupled to an SEM, which

allows for observing layering/banding (if present) within individual overgrowths (indicative of different cementation stages) (Fig. 7).

Quartz cement deposited during stages 1–3 is CL-luminescent, whereas quartz cement formed during the final stage is characteristically non-luminescent and qualitatively constitutes approx. one-half of the total cement volume (Fig. 7). In terms of $\delta^{18}\text{O}$ values, quartz cement zones 1, 3 and 4 fall between 24‰ and 21‰, and a mild tendency towards lower values is observed with each successive cement generation (Fig. 4e; Table 3). Quartz cement zone 2 is conspicuous in that $\delta^{18}\text{O}$ values abruptly break the trend defined by zones 1, 3 and 4 by transiently increasing to ~27.5‰ (Fig. 4e). For additional information on $\delta^{18}\text{O}$ zoning in quartz-overgrowths

Table 3

Isotopic composition ($\delta^{18}\text{O}$ by SIMS) of quartz-overgrowths in the upper Mt. Simon Sandstone (ADM Verification Well #1; depth = 1680.4 m/5513.2 ft). Refer to SA 1 for petrographic context of each spot-analysis.

Session specific sample I.D.	SIMS session	Sample region	Spot-size (μm)	$\delta^{18}\text{O}\text{‰}$ (VSMOW)	\pm (2SD)	QO Zone
20140224@372.asc	S4	Area 2	3	22.4	1.0	1
20140224@370.asc	S4	Area 2	3	23.6	1.0	1
20140224@357.asc	S4	Area 10	3	23.7	1.0	1
20140224@360.asc	S4	Area 10	3	22.7	1.0	1
20140224@359.asc	S4	Area 10	3	23.4	0.8	1
20140107@211.asc	S2	Area 1	10	28.5	0.5	2
20140107@210.asc	S2	Area 1	10	27.7	0.5	2
20140107@153.asc	S2	Area 2	10	27.4	0.5	2
20140107@179.asc	S2	Area 10	10	27.3	0.2	2
20140107@168.asc	S2	Area 4	10	27.5	0.3	2
20140513@610.asc	S7	Area 11	10	25.7	0.3	2
20140107@208.asc	S2	Area 1	10	21.5	0.5	3
20140107@166.asc	S2	Area 4	10	22.2	0.3	3
20140107@170.asc	S2	Area 4	10	23.2	0.3	3
20140513@621.asc	S7	Area 11	10	21.9	0.3	3
20140107@207.asc	S2	Area 1	10	21.1	0.5	4
20140107@214.asc	S2	Area 1	10	21.0	0.5	4
20140107@212.asc	S2	Area 1	10	22.0	0.5	4
20140107@213.asc	S2	Area 1	10	20.8	0.5	4
20140107@154.asc	S2	Area 2	10	21.2	0.5	4
20140224@369.asc	S4	Area 2	3	21.4	1.0	4
20140224@355.asc	S4	Area 10	3	21.3	0.8	4
20140224@356.asc	S4	Area 10	3	21.8	0.8	4
20140107@180.asc	S2	Area 10	10	21.3	0.2	4
20140513@608.asc	S7	Area 11	10	21.7	0.3	4
20140513@612.asc	S7	Area 11	10	22.0	0.3	4

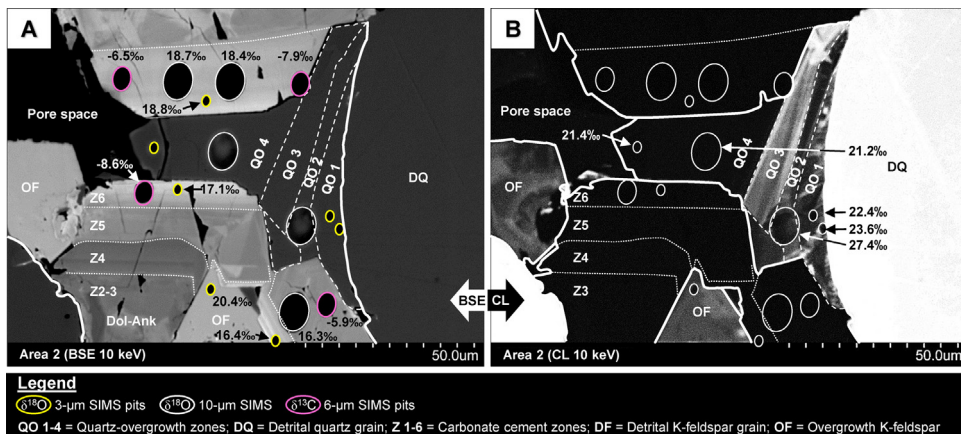


Fig. 7. (A and B) Corresponding BSE-SEM and CL-SEM images showing the microstratigraphic relationships among the different generations of quartz and carbonate cements identified within the upper Mt. Simon Sandstone (IBDP, ADM Verification Well#1, depth = 1680.4 m/5513.2 ft). Six major stages of carbonate cementation (Dol-Ank = dolomite-ankerite) and four distinct quartz-overgrowth (QO) generations were observed within the examined sample. DQ = detrital quartz; OF = overgrowth feldspar.

of the Mt. Simon Sandstone within the Illinois Basin, the interested reader is referred to the work of [Pollington et al. \(2011\)](#). No quartz-overgrowths were analyzed from the Eau Claire shale in the course of this study, but were previously examined by [Hyodo et al. \(2014\)](#).

3.4. Microstratigraphic relationships among cements (upper Mt. Simon Sandstone)

With regards to the microstratigraphic relationships among individual quartz-overgrowth and carbonate cements zones, we have observed the following (refer also to SA 1):

- 1) Based on an image analysis, dolomite-ankerite cement zones 1–4 comprise approx. 75% of the total carbonate cement volume (using ImageJ; [Schneider et al., 2012](#)). These four generations of cement precipitated before the onset of quartz cementation (Figs. 4f and 7; SA 1). Dolomite-ankerite zones 1–4 developed
- atop detrital quartz grain boundaries, which were free of any quartz-overgrowths at this stage of sediment lithification. Do note, however, that a portion of detrital quartz grains have partially corroded/embayed grain boundaries (see petrographic documentation in SA 1); in sample regions where this is evident, carbonate cements appear to locally replace quartz, but only to a limited extent ([Burley and Kantorowicz, 1986a, 1986b](#)). This type of texture predominates where detrital quartz grains are in contact with dolomite-ankerite cement zones 1–3, which, based on their mottled texture, appear to have recrystallized ([Machel, 1997](#)). Quartz-overgrowths are optically continuous with detrital cores, non-fibrous, and appear pristine. Where present, the underlying detrital quartz grain boundaries show no corroded textures.
- 2) The development of quartz-overgrowth zones 1 and 2 largely overlapped in time with the formation of carbonate cement zone 5 (Fig. 4f). However, a portion of carbonate cement zone 5 was

- already in place at the onset of QO zone 1 growth; this stage of carbonate cementation also continued for some time after QO zone 2 fully developed.
- 3) The development of quartz-overgrowth zones 3 and 4 largely overlapped in time with the development of carbonate cement zone 6 (Fig. 4f). However, a portion of QO zone 3 was already in place as carbonate cement zone 6 began forming, and this stage of carbonate cementation continued for some time after the end of QO zone 4 growth.

4. Discussion

The focus of the discussion that follows is two-fold: Part I is concerned with the IBDP site and simple predictions regarding possible $\delta^{13}\text{C}$ values for carbonate cements that are expected to form in response to long-term CO_2 storage. In Part II, we identify potential applications where carbonate isotope microanalysis by SIMS could contribute uniquely to research efforts concerned with geologic carbon storage. In keeping with the largely methodological theme of this article, a brief discussion on the evolution of isotope ratios in cements that formed during sediment burial and alteration at/near the IBDP site is provided as a supplement (SA 5).

4.1. Part I: Relevance to the Illinois Basin Decatur Project

Distinguishing carbonate mineral cements that form in response to CO_2 injection at the IBDP site from those that have formed naturally in response to prior, burial-related alteration of the sediment (diagenesis) would entail establishing a pre-injection petrographic baseline (one larger in scope than the small number of samples examined here) for the relevant carbonate-cemented intervals of the reservoir and basal caprock units. Such a baseline could be strongly reinforced by chemical and isotopic fingerprinting ($\delta^{13}\text{C}$ and $\delta^{18}\text{O}$). However, only small volumes of new carbonate are likely to form in the initial post-injection years, and so it may difficult to perform isotopic fingerprinting by conventional techniques, especially in the likely scenario where mechanical separation of new and preexisting cements will not be feasible. *In situ* isotope microanalysis by the SIMS technique offers a way past these technical obstacles.

Volumetrically significant occurrences of carbonate cement (predominantly dolomite-ankerite) locally occupy the pore space of the upper Mt. Simon Sandstone, nearby/within the gradational contact (Leetaru and Freiburg, 2014) with the overlying silty-shaly Eau Claire Fm. (Bowen et al., 2011; Fishman, 1997; Hoholick et al., 1984). Although somewhat limited in scope, our petrographic survey has additionally identified the presence of Mg-siderite cements in the upper Mt. Simon in samples from the basin margin in northern Illinois (relatively shallow burial environment; max. burial $\approx 1 \text{ km}/3500 \text{ ft}$; after Rowan et al., 2002) and at depth in the southern Illinois Basin (max burial $\approx 5.5 \text{ km}/18,000 \text{ ft}$; Figs. 1 and SA 1, Plate 24). While we did not observe such cements at the intermediate burial depths of this unit at the IBDP site, they have been documented in IBDP wells (e.g., Palkovic, 2015). Limited analyses indicate that carbonate minerals (calcite, dolomite) are also present in mudstone/shale interbeds at depth in the general vicinity of the CO_2 injection zone within the lower Mt. Simon Sandstone (e.g., see Table 8.3 in Finley, 2005). These clay mineral-rich interbeds are considered to be the first reactive environments that will be encountered by the emplaced CO_2 plume as it buoyantly rises through the reservoir, and are estimated to have the same capacity for sequestering carbon by mineral-trapping reactions as the basal Eau Claire shale (Finley, 2005). Isotopic fingerprinting could aid comparative studies of cements from these intervals in core material recovered at IBDP prior to injection (2011–2014) and in

sample material that may be recovered at some future time in the post-injection/monitoring phase currently underway. Such studies could aid in ground-truthing and/or refining reactive flow and transport models that attempt to: (1) predict the rate of mineral-trapping reactions, (2) to delimit the likely spatial distribution of reaction products (carbonate cements), and (3) to estimate the amount of CO_2 that will likely become permanently immobilized in mineral form (e.g., Liu et al., 2011). Note that whereas the injection zone is situated within the lower Mt. Simon Fm at the IBDP site, injection was also planned into the upper portion of this reservoir unit at the nearby site of the FutureGen 2.0 project (now defunded; e.g., Bonneville et al., 2013; Vermeul et al., 2016).

Within the diverse suite of lithofacies that comprise the Eau Claire shale, carbonate cements are generally abundant, although somewhat heterogeneously distributed (e.g., Finley, 2005; Neufelder et al., 2012; Palkovic, 2015; Śliwiński et al., 2016c). Carbon mineralization reactions are especially anticipated to occur along the reservoir-caprock interface, where reactive Fe-rich clay minerals and carbonate cements occur in abundance (Finley, 2005). Limited natural analogue studies indicate that chemical reactions between CO_2 and the caprock mineralogy can extend across a thickness of 10+ meters of the basal caprock layer (Bickle, 2009; Lu et al., 2009). During the initial post-injection pH buffering stage, carbonate cements in this basal layer may undergo partial to complete dissolution and subsequently re-precipitate higher within the unit (e.g., Kaldi et al., 2011). The depth of CO_2 penetration/reaction can generally be traced by means of $\delta^{13}\text{C}$ analysis (e.g., Lu et al., 2009), although the very small size of cement crystals in mudrocks/shales can complicate attempts at obtaining end-member signals from different carbonate components by means of conventional sampling/analytical techniques (e.g., Heinemann et al., 2013; Wilkinson et al., 2009).

A limited number of recent laboratory-scale experimental studies have investigated the reactivity of the IBDP reservoir and caprock units under simulated CO_2 storage conditions. Discernable changes in rock texture and mineralogy were noted within only a years' time, and indicate a tendency for dissolution of clay minerals that line the pore throats of the Mt. Simon Sandstone and for corrosion/degradation of illite, chlorite, K-feldspar, biotite and pyrite in the Eau Claire shale (Yokoujian et al., 2013). Iron-bearing clays were identified as a key reactant at IBDP, and are expected to help contribute the aqueous cations (Fe^{2+} , Mg^{2+}) necessary for carbon mineralization (Carroll et al., 2013; see also, e.g., Alemu et al., 2011; Kaldi et al., 2011). Reactive transport model simulations estimate that at least 10–20% of the introduced CO_2 may eventually be consumed in the precipitation of Fe-bearing carbonate cements (Liu et al., 2011), although this estimate would likely increase if the reactivity of Fe-rich clays with CO_2 -charged brine were taken into consideration (Carroll et al., 2013).

4.1.1. Forecasting $\delta^{13}\text{C}$ values for sequestration-related carbonates at IBDP

Here we make use of available data on reservoir conditions and the C-isotope ratio of the injected CO_2 at the IBDP site (e.g., Finley, 2005) to make simple predictions about the possible isotopic fingerprints of different carbonate cement types (e.g., calcite, dolomite-ankerite, siderite) that may form in response to long-term CO_2 storage.

Anticipated carbonate $\delta^{13}\text{C}$ values can be calculated using known temperature-dependent equilibrium isotope fractionation factors between the different common carbonate minerals and CO_2 (Table 4). The fractionation factor (α_{X-Y}) describes the difference in isotopic composition between two phases 'X' and 'Y':

$$\alpha_{X-Y} = R_X/R_Y = (\delta_X + 1000)/(\delta_Y + 1000) \quad (1)$$

Table 4

Predicted C-isotope composition of sequestration-related carbonate cements at the Illinois Basin Decatur Project site.

Equilibrium fractionation relationships: $10^3 \ln(\alpha_{\text{carbonate}} - \text{CO}_2) =$	Calibrated Range (°C)	$\delta^{13}\text{C}_{\text{CO}_2}$ (‰, VPDB)	Reservoir T(°C)	Predicted $\delta^{13}\text{C}_{\text{carbonate}}$ (‰, VPDB)
$2.53(10^6/T^2) - 20.20$ (^a siderite)	25–197 °C	-10	50	-6
$1.637(10^6/T^2) - 7.29$ (^b dol.)	100–250 °C	-10	50	-2
$1.648(10^6/T^2) - 8.02$ (^c calcite)	25–200 °C	-10	50	-2

^a Jimenez-Lopez and Romanek (2004): Using the results presented in Fig. 9a, specifically the linear trend that incorporates experimental results at 25 °C and those of Carothers et al. (1988) out to 197 °C, corrected for T and pH.

^b Eq. (6) of Horita (2014) (experimentally determined).

^c Chacko et al. (1991): Theoretical values from Table 7.

where R_X and R_Y represent the $^{13}\text{C}/^{12}\text{C}$ ratios for phases X and Y, respectively, whereas δ_X and δ_Y denote the per mil (‰) deviations of the $^{13}\text{C}/^{12}\text{C}$ ratios of phases X and Y in relation to a certified reference material (VPDB):

$$\delta_X = 1000 \times \left[\frac{R_X - R_{\text{VPDB}}}{R_{\text{VPDB}}} \right] \quad \& \quad \delta_Y = 1000 \times \left[\frac{R_Y - R_{\text{VPDB}}}{R_{\text{VPDB}}} \right] \quad (2)$$

Carbon isotope ratio measurements are expressed as a per mil (‰) deviation from the $^{13}\text{C}/^{12}\text{C}$ ratio of the VPDB international reference standard ($^{13}\text{C}/^{12}\text{C}_{\text{VPDB}} = 0.0112372$; Allison et al., 1995; Craig, 1957).

Fractionation factors (α_{X-Y}) are related to temperature via equations of the form:

$$1000 \times \ln(\alpha_{X-Y}) = \frac{A \times 10^6}{T^2} + B \cong \delta_X - \delta_Y \quad (3)$$

where T is the temperature in degrees Kelvin, whereas A and B are regressed parameters. Comprehensive reviews of these concepts can be found in Faure (1998) and Hoefs (2009).

Our calculations rely on the following constraints and assumptions: (1) The injected CO_2 plume becomes the dominant dissolved inorganic carbon (DIC) source in the storage system. The reservoir brine is initially acidified along zones of contact/interaction with the gradually expanding plume (however complex the interaction geometry may be; e.g., Johnson et al., 2004; Kampman et al., 2014). At some distance away from the injection site, silicate mineral dissolution reactions eventually establish pH conditions that are conducive to carbonate precipitation and provide the necessary divalent cations (e.g., Ca^{2+} , Mg^{2+} , Fe^{2+}). Note that as the plume continues to expand over centuries to millennia, the carbonate cement volume that may have formed at some distance by the end of the first post-injection decade, for example, should re-dissolve and re-precipitate further away (e.g., Liu et al., 2011). New cements are thus assumed to take on $\delta^{13}\text{C}$ values that reflect precipitation at an ambient reservoir temperature of ~50 °C (Labotka et al., 2015) and the $\delta^{13}\text{C}$ of the injected CO_2 (-9 to -11‰ at IBDP; Finley, 2005). Although the DIC pool in the IBDP reservoir has not been isotopically characterized, the low alkalinity of the Mt. Simon Formation brine (80 mg/L, as CaCO_3 ; Panno et al., 2013) suggests that upon interaction, the injected CO_2 will likely exert a primary control on the brine's isotopic composition. (2) The salinity/ionic composition of the reservoir brine (a Ca-Na-Cl type brine; Labotka et al., 2015) does not impart any secondary C-isotope fractionation effects during CO_2 dissolution. The current state of knowledge indicates that the influence of salinity on C-isotope partitioning between $\text{CO}_2(g)$ and DIC (i.e., the 'salt-effect') is negligible (however this is not the case for O-isotopes); while studies in this field are still somewhat limited, Mayer et al. (2015) observe that "there is currently no evidence that these effects would significantly compromise the suitability of the stable isotopic composition of injected CO_2 as a tracer tool."

Using available data on carbon isotope partitioning between carbonates and $\text{CO}_2(g)$ (Table 4), we calculate the following approximate $\delta^{13}\text{C}$ values for sequestration-related cements: -2‰ VPDB for

calcite (based on the work of Chacko et al., 1991), -6‰ for siderite (after Jimenez-Lopez and Romanek, 2004), and -2‰ for dolomite-ankerite (based on the recent experimental work of Horita (2014) for end-member dolomite; Fig. 3). A fractionation factor between $\text{CO}_2(g)$ and ankerite of any composition has not yet been experimentally calibrated, and it thus remains unknown how iron affects equilibrium relations relative to end-member dolomite. (Note that carbonate $\delta^{18}\text{O}$ values cannot be forecast at present because, to our knowledge, the $\delta^{18}\text{O}$ of the supercritical CO_2 stream at the IBDP site has not been determined/reported, although brine $\delta^{18}\text{O}$ values are known for various depths within the reservoir unit; e.g., Labotka et al., 2015).

How would these values be affected by primary carbonate cement dissolution and mixing of the resulting $\delta^{13}\text{C}$ signal with that of the injected CO_2 ? At present we can only assess the potential impact on newly formed dolomite, as calcite and siderite cements were not isotopically characterized as part of this study (neither calcite nor siderite were encountered in the small sample suite examined, although both are known constituents of the reservoir mineralogy; e.g., Palkovic, 2015). A bulk weighted average $\delta^{13}\text{C}$ value of -2.5‰ VPDB was calculated for the representative patch of primary dolomite-ankerite cement shown in Fig. 3b. An image analysis (using ImageJ software; Schneider et al., 2012) was performed to estimate the volume fraction represented by each cement zone (Zones 1, 2 and 3 together comprise 55% of the total volume, whereas zones 4, 5 and 6 respectively comprise 20%, 15% and 10%). Rapid and complete dissolution of this cement volume at 50 °C would, under the experimental conditions described by Horita (2014), produce $\text{CO}_2(g)$ with a $\delta^{13}\text{C}$ value -11‰ VPDB. Thus, the impact of primary cement dissolution may not be discernable considering that the $\delta^{13}\text{C}$ of the injected CO_2 stream falls between -9 to -11‰ VPDB.

4.2. Part II: Broader applications

Here we attempt to identify some areas of current research interest where *in situ* isotope microanalysis by SIMS could provide potentially unique insights to investigations concerned with understanding how CO_2 will interact with geological reservoirs and caprocks under engineered storage conditions. These include:

► Identifying sequestration-related carbonate cements in engineered CO_2 -storage reservoirs

Only small cement volumes are anticipated in the initial years post-injection. Nonetheless, as little as 3 micrometers (μm) of new growth could be readily analyzed by the methodology described here, thus potentially providing early inputs for calibrating geochemical models that attempt to predict how the mineralogy of a given reservoir-caprock system will evolve in the long-term in response to imposed CO_2 storage (and to derive more accurate estimates regarding the fraction of CO_2 that will become securely trapped in mineral form over time). Hypothetically, it may also be necessary in future monitoring studies at CCS sites to verify, via isotopic fingerprinting, whether fracture-filling cements in caprock units are related to CO_2 leakage.

►Characterizing the carbonate components that pre-date CO₂-charging of natural and/or engineered reservoirs

Naturally-occurring accumulations of CO₂ in geological environments are helping to build an understanding of how CO₂ interacts in the long-term (10⁵–10⁶ years) with reservoir-caprock systems (e.g., Bickle et al., 2013). Studies of these so-called natural analogues aid, for example, in: (1) identifying the dominant fluid-mineral reactions that are expected to occur during engineered CO₂ storage; (2) allow for estimating rates of carbon mineralization; and (3) provide a means of calibrating geochemical models and reservoir simulations against the natural world (e.g., Bickle et al., 2013; Higgs et al., 2015; Pearce et al., 1996; Sathaye et al., 2014; Stevens et al., 2001; Watson et al., 2004). As they relate to carbon sequestration in deep saline aquifers, the above three points have been identified as general knowledge gaps by the IPCC Special Report on CO₂ Capture and Storage (2005) (Michael et al., 2009). It was noted in a recent review of natural analogues that “a complete model of the fluid-mineral reactions will require both modeling of changes in fluid chemistry in conjunction with a full understanding of the petrology of the sandstone aquifer in which it will be essential to distinguish reaction products related to the present phase of [CO₂-charge related] alteration from earlier detrital and diagenetic phases” (Bickle et al., 2013). This point extends in relevance to the problem of determining the depth to which CO₂ penetrates into the caprock units that overlie natural reservoirs (as a means of assessing the likely long-term integrity of reservoir seals). Carbonate δ¹³C and δ¹⁸O signatures are a well-established tracer, although the ability of conventional methods to fully resolve isotopic differences among different end-member components can be hindered by small crystal size (e.g., Lu et al., 2009) and/or if chemo-isotopic zonation is present at the micrometer scale (Heinemann et al., 2013; Wilkinson et al., 2009).

►Characterizing experimental reaction products

This includes assessments of reservoir/caprock reactivity under simulated CO₂-storage conditions in cases where reaction product volumes are too small for conventional isotope ratio measurements. A further example is the problem of constraining equilibrium isotope fractionation factors between fluids and minerals during precipitation. In experiments conducted at temperatures relevant to CO₂ storage in saline aquifers (~50–150 °C), precipitation rates are frustratingly slow for most common minerals. Reaction product volumes that form over reasonable laboratory time-scales (months to several years) are consequently quite small, as for example micrometer-scale overgrowths in instances where seed crystals are used to stimulate mineral growth (e.g., Pollington et al., 2016).

►Determining the carbon source(s) involved in carbonate cement-forming reactions in sequestration environments other than deep saline aquifers

Broadly speaking, many of the carbon sequestration strategies currently under consideration (e.g., Power et al., 2013) seek efficient means (process routes) of converting CO₂ gas into carbonate minerals. Carbon mineralization results in a product that is both environmentally benign and stable over geological time scales. The fundamental idea underlying many strategies is essentially one of mimicking natural geological processes (e.g., silicate mineral weathering reactions or microbial mineralization) and devising efficient engineering solutions aimed at accelerating the rate at which these processes operate in controlled settings. Although such sequestration concepts are still in the basic research and development stage, research efforts to date indicate that they could be effective in substantially offsetting annual anthropogenic CO₂ emissions if deployed in tandem on a sufficiently large scale. *In situ* carbonation of peridotite is one such strategy (e.g., Kelemen et al., 2011; Kelemen and Matter, 2008; Lackner et al., 1995; Matter and Kelemen, 2009). Promoting the carbonation of ultramafic mine

tailings is another (e.g., Wilson et al., 2006, 2009). It has been estimated, for example, that the annual sequestration capacity of a large mine can exceed its annual CO₂ emissions (Power et al., 2013; Wilson et al., 2006).

Abundant in ultramafic mine tailings are Ca-Mg-Fe-rich silicate minerals (e.g., olivine, pyroxene, plagioclase feldspars) that are thermodynamically unstable at Earth surface conditions; consequently, they weather rapidly. Carbonate minerals, particularly various forms of hydrated Mg-carbonates (e.g., nesquehonite, dypingite, hydromagnesite, etc.), are among the common reaction products, forming crusts that may exhibit mineralogical and/or stable carbon isotope zonation (Wilson et al., 2006). In the case of micrometer-scale mineralogical banding, δ¹³C zonation could reflect differences in the degree to which different hydrated Mg-carbonate species fractionate the stable isotopes of carbon during precipitation. It has also been recognized that different varieties of hydrated Mg-carbonates likely form via distinctly different pathways; some may be entirely abiotic in origin, whereas the precipitation of others may be microbially-mediated (Ferris et al., 1994; Power and Southam, 2005; Wilson et al., 2009). Understanding the relative efficiency of these end-member modes is significant for engineering efficient carbon mineralization systems, which may in the future rely in-part on microbial organisms that have been modified to locally accelerate the rate of silicate weathering and/or carbonate precipitation (Cappuccio et al., 2012; Chen et al., 2012; Ferris et al., 1994; Kamennaya et al., 2012; Krieger, 2012; Power et al., 2013). To this end, stable carbon and oxygen isotopic data, when used together with quantitative mineralogical analyses, can be an effective tool for identifying the carbon source(s) tapped during the formation of carbonate crusts (e.g., atmospheric or biologically cycled CO₂, or carbon derived from dissolution of carbonate minerals in bedrock) and for quantifying the rate of their formation (e.g., Wilson et al., 2009).

5. Concluding remarks

Stable carbon and oxygen isotope analyses (δ¹³C and δ¹⁸O, respectively) are an important component of research into CO₂-sequestration strategies, especially in so-called natural analogues studies. Research efforts directed at natural analogues seek in-part to quantify the rate and extent of CO₂-trapping via carbonate mineral cement formation (*i.e.*, carbon mineralization or mineral-trapping of CO₂), and by so doing to make/refine quantitative predictions about the probable long-term fate of CO₂ in prospective engineered reservoirs. Isotopic signatures (or fingerprints) provide a means by which to distinguish different carbonate components present in the reservoir-caprock system (*i.e.*, those that pre-date from those that post-date CO₂-charging).

However, clear interpretations of isotopic data acquired *via* conventional sampling techniques in isotope ratio mass spectrometry (IRMS) (sampling typically at the 100–1000 μm scale) can be significantly hindered in situations where it is not possible to mechanically or chemically separate different carbonate components (due to small crystal size and/or the presence of chemo-isotopic zoning at the micrometer scale).

Advances in secondary ion mass spectrometer (SIMS) instrument design, analytical techniques and standardization have brought about the capability to routinely perform δ¹⁸O and δ¹³C measurements *in situ* from sample domains as small as 1–10 μm across, with preservation of the petrographic context of the analyzed sample volume. Many of the common Ca-Mg-Fe carbonates can now be accurately analyzed, including the full spectrum of compositions along the dolomite-ankerite and magnesite-siderite solid-solution series. These advances – many of which have occurred since the time when geologic carbon sequestration was

first proposed in the mid-1990's (Bachu et al., 1994; Lackner et al., 1995) and research into natural analogues began (Pearce et al., 1996) – expand the potential analytical toolkit available to the research community concerned with developing effective carbon sequestration strategies.

The analytical capability described here could provide potentially unique insights when applied in studies concerned, for example, with following objectives (although this remains to be critically evaluated):

- Verifying if, where, and at what rate carbonate cements precipitate in geological reservoirs designated for engineered CO₂ storage;
- Characterizing the isotopic composition of carbonate components that pre-date the CO₂-charge in engineered reservoirs or their natural analogues;
- Determining or refining existing rate estimates (based on bulk isotope analyses) of carbonate cement-forming reactions in a variety of natural analogue environments;
- Analyzing the isotopic composition of experimental reaction products in instances where product volumes are sufficiently small so as to hinder analysis by conventional IRMS methods (this applies to laboratory-scale experiments designed to elucidate how CO₂ interacts with representative rock samples from a given reservoir-caprock system).

Acknowledgments

This material is based primarily upon work supported by the US Department of Energy Office of Science, Office of Basic Energy Sciences, Chemical Sciences, Geosciences, and Biosciences Division under award number DE-FG02-93ER14389. The WiscSIMS Laboratory is partly funded by the US National Science Foundation (EAR-1355590). We thank our colleagues at the University of Wisconsin-Madison for providing instrumentation support: N. Kita (SIMS), J. Kern (SIMS), J. Fournelle (SEM & EPMA) and P. Gopon (SEM & EPMA). The Midwest Geological Sequestration Consortium is acknowledged for making samples from the Illinois Basin Decatur Project (IBDP) available for study and we thank A. Hyodo and the staff of the Illinois State Geological Survey for assistance with sampling. We also thank I. Power for providing feedback and two anonymous reviewers for a thoughtful and constructive assessment of this work.

Appendix A. Supplementary data

Supplementary data associated with this article can be found, in the online version, at <http://dx.doi.org/10.1016/j.ijggc.2016.12.013>.

References

- Alemu, B.L., Aagaard, P., Munz, I.A., Skurtveit, E., 2011. Caprock interaction with CO₂: a laboratory study of reactivity of shale with supercritical CO₂ and brine. *Appl. Geochem.* 26, 1975–1989, <http://dx.doi.org/10.1016/j.apgeochem.2011.06.028>.
- Allison, C.E., Francy, R.J., Meijer, H.A.J., 1995. Recommendations for the reporting of stable isotope measurements of carbon and oxygen in CO₂ gas. In: Reference and Intercomparison Materials for Stable Isotopes of Light Elements. Presented at the Reference and Intercomparison Materials for Stable Isotopes of Light Elements. International Atomic Energy Agency, Vienna, Austria, pp. 155–162.
- Bachu, S., Gunter, W.D., Perkins, E.H., 1994. Aquifer disposal of CO₂: hydrodynamic and mineral trapping. *Energy Convers. Manag.* 35, 269–279, [http://dx.doi.org/10.1016/0196-8904\(94\)90060-4](http://dx.doi.org/10.1016/0196-8904(94)90060-4).
- Baines, S.J., Worden, R.H., 2004a. Geological storage of carbon dioxide. *Geol. Soc. Lond. Spec. Publ.* 233, 1–6.
- Baines, S.J., Worden, R.H., 2004b. The long-term fate of CO₂ in the subsurface: natural analogues for CO₂ storage. *Geol. Soc. Lond. Spec. Publ.* 233, 59–85.
- Bickle, M., Kampman, N., Wigley, M., 2013. Natural analogues. *Rev. Mineral. Geochem.* 77, 15–71, <http://dx.doi.org/10.2138/rmg.2013.77.2>.
- Bickle, M.J., 2009. Geological carbon storage. *Nat. Geosci.* 2, 815–818, <http://dx.doi.org/10.1038/ngeo687>.
- Bonneville, A., Gilmore, T., Sullivan, C., Vermeul, V., Kelley, M., White, S., Appriou, D., Bjornstad, B., Gerst, J., Gupta, N., Horner, J., McNeil, C., Moody, M., Rike, W., Spane, F., Thorne, P., Zeller, E., Zhang, F., Hoffmann, J., Humphreys, K., 2013. Evaluating the suitability for CO₂ storage at the FutureGen 2.0 site, Morgan County, Illinois, USA. *Energy Procedia* 37, 6125–6132, <http://dx.doi.org/10.1016/j.egypro.2013.06.541>.
- Bowen, B.B., Ochoa, R.I., Wilkens, N.D., Brophy, J., Lovell, T.R., Fischietto, N., Medina, C.R., Rupp, J.A., 2011. Depositional and diagenetic variability within the Cambrian Mount Simon Sandstone: implications for carbon dioxide sequestration. *Environ. Geosci.* 18, 69–89, <http://dx.doi.org/10.1306/eg.07271010012>.
- Burley, S.D., Kantorowicz, J.D., 1986a. Thin section and SEM textural criteria for the recognition of cement-dissolution porosity in sandstones. *Sedimentology* 33, 587–604.
- Burley, S.D., Kantorowicz, J.D., 1986b. Reply. *Sedimentology* 33, 608–614, <http://dx.doi.org/10.1111/j.1365-3091.1986.tb00765.x>.
- Cappuccio, J.A., Lui, G.V., Pillar, V.D., Ajo-Franklin, C.M., 2012. Tuning microbial surfaces to control carbonate mineralization. *Biophys. J.* 102, 188a, <http://dx.doi.org/10.1016/j.bpj.2011.11.1024>.
- Carroll, S.A., McNab, W.W., Dai, Z., Torres, S.C., 2013. Reactivity of Mount Simon Sandstone and the Eau Claire Shale under CO₂ storage conditions. *Environ. Sci. Technol.* 47, 252–261, <http://dx.doi.org/10.1021/es301269k>.
- Carothers, W.W., Adami, L.H., Rosenbauer, R.J., 1988. Experimental oxygen isotope fractionation between siderite-water and phosphoric acid liberated CO₂-siderite. *Geochim. Cosmochim. Acta* 52, 2445–2450.
- Celia, M.A., Bachu, S., Nordbotten, J.M., Bandilla, K.W., 2015. Status of CO₂ storage in deep saline aquifers with emphasis on modeling approaches and practical simulations. *Water Resour. Res.* 51, 6846–6892, <http://dx.doi.org/10.1002/2015WR017609>.
- Chacko, T., Mayeda, T.K., Clayton, R.N., Goldsmith, J.R., 1991. Oxygen and carbon isotope fractionations between CO₂ and calcite. *Geochim. Cosmochim. Acta* 55, 2867–2882, [http://dx.doi.org/10.1016/0016-7037\(91\)90452-B](http://dx.doi.org/10.1016/0016-7037(91)90452-B).
- Chang, L.L., Howie, R.A., Zussman, J., 1998. *Non-Silicates: Sulphates, Carbonates, Phosphates Halides*. Longman Group Limited, Harlow, p. 383.
- Chen, P.-H., Liu, H.-L., Chen, Y.-J., Cheng, Y.-H., Lin, W.-L., Yeh, C.-H., Chang, C.-H., 2012. Enhancing CO₂ bio-mitigation by genetic engineering of cyanobacteria. *Energy Environ. Sci.* 5, 8318–8327, <http://dx.doi.org/10.1039/c2ee21124f>.
- Craig, H., 1957. Isotopic standards for carbon and oxygen and correction factors for mass-spectrometric analysis of carbon dioxide. *Geochim. Cosmochim. Acta* 12, 133–149.
- DOE, 2010. Carbon sequestration ATLAS of the United States and Canada. Off. Foss. Energy Natl. Energy Technol. Lab. Morgant. WV 90p.
- DePaolo, D.J., Cole, D.R., 2013. Geochemistry of geologic carbon sequestration: an overview. *Rev. Mineral. Geochem.* 77, 1–14, <http://dx.doi.org/10.2138/rmg.2013.77.1>.
- Eiler, J.M., Valley, J.W., Graham, C.M., 1997. Standardization of SIMS analysis of O and C isotope ratios in carbonates from ALH84001. Lunar and Planetary Science Conference, p. 327.
- Faure, G., 1998. *Principles and Applications of Geochemistry: A Comprehensive Textbook for Geology Students*. Prentice Hall.
- Ferris, F., Wiese, R., Fyfe, W., 1994. Precipitation of carbonate minerals by microorganisms—implications for silicate weathering and the global carbon-dioxide budget. *Geomicrobiol. J.* 12, 1–13.
- Finley, R., 2005. *An Assessment of Geological Carbon Sequestration Options in the Illinois Basin*. Department of Energy, United States.
- Fishman, N.S., 1997. Basin-wide fluid movement in a Cambrian paleoaquifer: evidence from the Mt. Simon Sandstone, Illinois and Indiana. In: Montanez, I.P., Gregg, J.M., Shelton, K.L. (Eds.), *Basin-Wide Diagenetic Patterns: Integrated Petrologic, Geochemical, and Hydrologic Considerations*. SEPM (Society for Sedimentary Geology), Tulsa, Oklahoma, U.S.A, pp. 221–234.
- Gale, J., 2004. Why do we need to consider geological storage of CO₂. *Geol. Soc. Lond. Spec. Publ.* 233, 7–15, <http://dx.doi.org/10.1144/GSL.SP.2004.233.01.02>.
- Gibbins, J., Chalmers, H., 2008. Carbon capture and storage. *Energy Policy* 36, 4317–4322, <http://dx.doi.org/10.1016/j.enpol.2008.09.058>.
- Gunter, W.D., Bachu, S., Benson, S., 2004. The role of hydrogeological and geochemical trapping in sedimentary basins for secure geological storage of carbon dioxide. *Geol. Soc. Lond. Spec. Publ.* 233, 129–145.
- Haszeldine, R.S., Quinn, O., England, G., Wilkinson, M., Shipton, Z.K., Evans, J.P., Heath, J., Crossey, L., Ballantine, C.J., Graham, C.M., 2005. Natural geochemical analogues for carbon dioxide storage in deep geological porous reservoirs, a United Kingdom perspective. *Oil Gas Sci. Technol.* 60, 33–49.
- Heinemann, N., Wilkinson, M., Haszeldine, R.S., Fallick, A.E., Pickup, G.E., 2013. CO₂ sequestration in a UK North Sea analogue for geological carbon storage. *Geology* 41, 411–414, <http://dx.doi.org/10.1130/G33835.1>.
- Hervig, R.L., Williams, P., Thomas, R.M., Schauer, S.N., Steele, I.M., 1992. Microanalysis of oxygen isotopes in insulators by secondary ion mass spectrometry. *Int. J. Mass Spectrom. Ion Process.* 120, 45–63.
- Higgs, K.E., Haese, R.R., Golding, S.D., Schacht, U., Watson, M.N., 2015. The Pretty Hill formation as a natural analogue for CO₂ storage: an investigation of mineralogical and isotopic changes associated with sandstones exposed to low, intermediate and high CO₂ concentrations over geological time. *Chem. Geol.* 399, 36–64, <http://dx.doi.org/10.1016/j.chemgeo.2014.10.019>, Measuring and predicting the geochemical impacts of CO₂ storage on reservoir rocks.

- Hoefs, J., 2009. *Stable Isotope Geochemistry*, 6th ed. Springer-Verlag, Berlin, Heidelberg.
- Hoffert, M.I., Caldeira, K., Benford, G., Criswell, D.R., Green, C., Herzog, H., Jain, A.K., Kheshgi, H.S., Lackner, K.S., Lewis, J.S., et al., 2002. Advanced technology paths to global climate stability: energy for a greenhouse planet. *Science* 298, 981–987.
- Hoholick, J.D., Metarko, T., Potter, P.E., 1984. Regional variations of porosity and cement: St. Peter and Mount Simon sandstones in Illinois Basin. *AAPG Bull.* 68, 753–764.
- Horita, J., 2014. Oxygen and carbon isotope fractionation in the system dolomite–water–CO₂ to elevated temperatures. *Geochim. Cosmochim. Acta* 129, 111–124, <http://dx.doi.org/10.1016/j.gca.2013.12.027>.
- Hosa, A., Esentia, M., Stewart, J., Haszeldine, S., 2011. Injection of CO₂ into saline formations: benchmarking worldwide projects. *Chem. Eng. Res. Des.* 89, 1855–1864, <http://dx.doi.org/10.1016/j.cherd.2011.04.003>.
- Hyodo, A., Kozdon, R., Pollington, A.D., Valley, J.W., 2014. Evolution of quartz cementation and burial history of the Eau Claire Formation based on in situ oxygen isotope analysis of quartz overgrowths. *Chem. Geol.* 384, 168–180, <http://dx.doi.org/10.1016/j.chemgeo.2014.06.021>.
- IPCC, 2005. *Special Report on Carbon Dioxide Capture and Storage*. Cambridge University Press, for the Intergovernmental Panel on Climate Change, Cambridge.
- Jimenez-Lopez, C., Romanek, C.S., 2004. Precipitation kinetics and carbon isotope partitioning of inorganic siderite at 25 °C and 1 atm. *Geochim. Cosmochim. Acta* 68, 557–571, [http://dx.doi.org/10.1016/S0016-7037\(03\)00460-5](http://dx.doi.org/10.1016/S0016-7037(03)00460-5).
- Johnson, J.W., Nitao, J.J., Knauss, K.G., 2004. Reactive transport modelling of CO₂ storage in saline aquifers to elucidate fundamental processes, trapping mechanisms and sequestration partitioning. *Geol. Soc. Lond.* 233, 107–128, Special Publications.
- Kaldi, J., Daniel, R., Tenthorey, E., Michael, L., Schacht, U., Nicol, A., Undershultz, J., Backé, G., 2011. *Caprock Systems for CO₂ Geological Storage*. Cooperative Research Centre for Greenhouse Gas Technologies, Canberra, ACT, CO2CRC Publication Number RPT10–2774.
- Kamennaya, N., Ajo-Franklin, C., Northen, T., Jansson, C., 2012. Cyanobacteria as biocatalysts for carbonate mineralization. *Minerals* 2, 338–364, <http://dx.doi.org/10.3390/min2040338>.
- Kampman, N., Bickle, M., Wigley, M., Dubacq, B., 2014. Fluid flow and CO₂–fluid–mineral interactions during CO₂ storage in sedimentary basins. *Chem. Geol.* 369, 22–50, <http://dx.doi.org/10.1016/j.chemgeo.2013.11.012>.
- Kelemen, P.B., Matter, J., 2008. In situ carbonation of peridotite for CO₂ storage. *Proc. Natl. Acad. Sci.* 105, 17295–17300.
- Kelemen, P.B., Matter, J., Streit, E.E., Rudge, J.F., Curry, W.B., Blusztajn, J., 2011. Rates and mechanisms of mineral carbonation in peridotite: natural processes and recipes for enhanced, in situ CO₂ capture and storage. *Annu. Rev. Earth Planet. Sci.* 39, 545–576, <http://dx.doi.org/10.1146/annurev-earth-092010-152509>.
- Kelly, J.L., Fu, B., Kita, N.T., Valley, J.W., 2007. Optically continuous silcrete quartz cements of the St. Peter Sandstone: high precision oxygen isotope analysis by ion microprobe. *Geochim. Cosmochim. Acta* 71, 3812–3832, <http://dx.doi.org/10.1016/j.gca.2007.05.014>.
- Kita, N.T., Ushikubo, T., Fu, B., Valley, J.W., 2009. High precision SIMS oxygen isotope analysis and the effect of sample topography. *Chem. Geol.* 264, 43–57.
- Kolata D.R., 2005. Bedrock geology of Illinois. Illinois Map 14.
- Kolata, D.R., Nimz, C.K., 2010. *Geology of Illinois*. University of Illinois at Urbana-Champaign, Institute of Natural Resource Sustainability, Illinois State Geological Survey, Champaign, Illinois.
- Krieger, K., 2012. Genetically Engineered Bacteria Could Help Fight Climate Change [WWW Document], URL <http://www.sciencemag.org/news/2012/02/genetically-engineered-bacteria-could-help-fight-climate-change> (Accessed 3 August 2016).
- Labotka, D.M., Panno, S.V., Locke, R.A., Freiburg, J.T., 2015. Isotopic and geochemical characterization of fossil brines of the Cambrian Mt. Simon Sandstone and Ironton–Galesville Formation from the Illinois Basin, USA. *Geochim. Cosmochim. Acta* 165, 342–360, <http://dx.doi.org/10.1016/j.gca.2015.06.013>.
- Lackner, K.S., Wendt, C.H., Butt, D.P., Joyce Jr., E.L., Sharp, D.H., 1995. Carbon dioxide disposal in carbonate minerals. *Energy* 20, 1153–1170, [http://dx.doi.org/10.1016/0360-5442\(95\)00071-N](http://dx.doi.org/10.1016/0360-5442(95)00071-N).
- Lackner, K.S., 2003. A guide to CO₂ sequestration. *Science* 300, 1677–1678.
- Leetar, H.E., Freiburg, J.T., 2014. Litho-facies and reservoir characterization of the Mt. Simon sandstone at the Illinois Basin – Decatur Project: litho-facies and reservoir characterization of the Mt. Simon Sandstone at the Illinois Basin. *Greenh. Gases Sci. Technol.* 4, 580–595, <http://dx.doi.org/10.1002/ghg.1453>.
- Leetar, H.E., Frailey, S., Morse, D., Finley, R.J., Rupp, J.A., Drahovzal, J.A., McBride, J.H., 2009. *Carbon Sequestration in the Mt. Simon Sandstone Saline Reservoir*.
- Liu, F., Lu, P., Zhu, C., Xiao, Y., 2011. Coupled reactive flow and transport modeling of CO₂ sequestration in the Mt. Simon Sandstone formation, Midwest U.S.A. *Int. J. Greenh. Gas Control* 5, 294–307, <http://dx.doi.org/10.1016/j.ijggc.2010.08.008>.
- Lu, J., Wilkinson, M., Haszeldine, R.S., Fallick, A.E., 2009. Long-term performance of a mudrock seal in natural CO₂ storage. *Geology* 37, 35–38, <http://dx.doi.org/10.1130/G25412A.1>.
- Lu, J., Wilkinson, M., Haszeldine, R.S., Boyce, A.J., 2011. Carbonate cements in Miller field of the UK North Sea: a natural analog for mineral trapping in CO₂ geological storage. *Environ. Earth Sci.* 62, 507–517, <http://dx.doi.org/10.1007/s12665-010-0543-1>.
- Machel, H.G., 1997. Recrystallization versus neomorphism, and the concept of significant recrystallization in dolomite research. *Sediment. Geol.* 113, 161–168.
- Matter, J.M., Kelemen, P.B., 2009. Permanent storage of carbon dioxide in geological reservoirs by mineral carbonation. *Nat. Geosci.* 2, 837–841, <http://dx.doi.org/10.1038/ngeo683>.
- Matter, J.M., Stute, M., Snæbjörnsdóttir, S.Ó., Oelkers, E.H., Gislason, S.R., Aradottir, E.S., Sigfusson, B., Gunnarsson, I., Sigurdardóttir, H., Gunnlaugsson, E., Axelsson, G., Alfredsson, H.A., Wolff-Boenisch, D., Mesfin, K., Taya, D.F., de la R., Hall, J., Dideriksen, K., Broecker, W.S., 2016. Rapid carbon mineralization for permanent disposal of anthropogenic carbon dioxide emissions. *Science* 352, 1312–1314, <http://dx.doi.org/10.1126/science.aad8132>.
- Mayer, B., Humez, P., Becker, V., Dalkhaa, C., Rock, L., Myrttinen, A., Barth, J.A.C., 2015. Assessing the usefulness of the isotopic composition of CO₂ for leakage monitoring at CO₂ storage sites: a review. *Int. J. Greenh. Gas Control* 37, 46–60, <http://dx.doi.org/10.1016/j.ijggc.2015.02.021>.
- McGrail, B.P., Schaeff, H.T., Ho, A.M., Chien, Y.-J., Dooley, J.J., Davidson, C.L., 2006. Potential for carbon dioxide sequestration in flood basalts. *J. Geophys. Res. Solid Earth* 111, 1–13.
- McGrail, B.P., Schaeff, H.T., Spane, F.A., Cliff, J.B., Qafoku, O., Horner, J.A., Thompson, C.J., Owen, A.T., Sullivan, C.E., 2016. Field validation of supercritical CO₂ reactivity with basalts. *Environ. Sci. Technol. Lett.*, <http://dx.doi.org/10.1021/acs.estlett.6b00387>.
- Michael, K., Arnott, M., Cook, P., Ennis-King, J., Funnell, R., Kaldi, J., Kirste, D., Paterson, L., 2009. CO₂ storage in saline aquifers I—current state of scientific knowledge. *Energy Procedia* 1, 3197–3204, <http://dx.doi.org/10.1016/j.egypro.2009.02.103>.
- Michael, K., Golab, A., Shulakova, V., Ennis-King, J., Allinson, G., Sharma, S., Aiken, T., 2010. Geological storage of CO₂ in saline aquifers—a review of the experience from existing storage operations. *Int. J. Greenh. Gas Control* 4, 659–667, <http://dx.doi.org/10.1016/j.ijggc.2009.12.011>.
- Morad, S., 2009. *Carbonate Cementation in Sandstones: Distribution Patterns and Geochemical Evolution* (Special Publication 26 of the IAS). John Wiley & Sons.
- Neufelder, R.J., Bowen, B.B., Lahann, R.W., Rupp, J.A., 2012. Lithologic, mineralogical, and petrophysical characteristics of the Eau Claire Formation: complexities of a carbon storage system seal. *Environ. Geosci.* 19, 81–104, <http://dx.doi.org/10.1306/eg.02081211014>.
- Orr, F.M., 2009. CO₂ capture and storage: are we ready? *Energy Environ. Sci.* 2, 449–458, <http://dx.doi.org/10.1039/b2822107n>.
- Page, F.Z., Ushikubo, T., Kita, N.T., Riciputi, L.R., Valley, J.W., 2007. High-precision oxygen isotope analysis of picogram samples reveals 2 μm gradients and slow diffusion in zircon. *Am. Mineral.* 92, 1772–1775, <http://dx.doi.org/10.2138/am.2007.2697>.
- Palkovic, M.J., 2015. *Depositional Characterization of the Eau Claire Formation at the Illinois Basin-Decatur Project: Facies, Mineralogy and Geochemistry (M.Sc.) University of Illinois at Urbana-Champaign*.
- Panno, S.V., Hackley, K.C., Locke, R.A., Krapac, I.G., Wimmer, B., Iranmanesh, A., Kelly, W.R., 2013. Formation waters from Cambrian-age strata, Illinois Basin, USA: constraints on their origin and evolution. *Geochim. Cosmochim. Acta* 122, 184–197, <http://dx.doi.org/10.1016/j.gca.2013.08.021>.
- Pearce, J.M., Holloway, S., Wacker, H., Nelis, M.K., Rochelle, C., Bateman, K., 1996. Natural occurrences as analogues for the geological disposal of carbon dioxide. *Energy Convers. Manag.*, Proceedings of the International Energy Agency Greenhouse Gases: Mitigation Options Conference 37, 1123–1128, [http://dx.doi.org/10.1016/0196-8904\(95\)00309-6](http://dx.doi.org/10.1016/0196-8904(95)00309-6).
- Pollington, A.D., Kozdon, R., Valley, J.W., 2011. Evolution of quartz cementation during burial of the Cambrian Mount Simon Sandstone, Illinois Basin: in situ microanalysis of δ¹⁸O. *Geology* 39, 1119–1122.
- Pollington, A.D., Kozdon, R., Anovitz, L.M., Georg, R.B., Spicuzza, M.J., Valley, J.W., 2016. Experimental calibration of silicon and oxygen isotope fractionations between quartz and water at 250 °C by in situ microanalysis of experimental products and application to zoned low δ³⁰Si quartz overgrowths. *Chem. Geol.* 421, 127–142, <http://dx.doi.org/10.1016/j.chemgeo.2015.11.011>.
- Power, I., Southam, G., 2005. Carbon dioxide sequestration through enhanced weathering of chrysotile mine tailings and subsequent microbial precipitation of magnesium carbonates. *Geochim. Cosmochim. Acta*, 834.
- Power, I.M., Harrison, A.L., Dipple, G.M., Wilson, S.A., Kelemen, P.B., Hitch, M., Southam, G., 2013. Carbon mineralization: from natural analogues to engineered systems. *Rev. Mineral. Geochem.* 77, 305–360, <http://dx.doi.org/10.2138/rmg.2013.77.9>.
- Rowan, E.L., Goldhaber, M.B., Hatch, J.R., 2002. Regional fluid flow as a factor in the thermal history of the Illinois Basin: constraints from fluid inclusions and the maturity of Pennsylvanian coals. *AAPG Bull.* 86, 257–277.
- Sathaye, K.J., Hesse, M.A., Cassidy, M., Stockli, D.F., 2014. Constraints on the magnitude and rate of CO₂ dissolution at Bravo Dome natural gas field. *Proc. Natl. Acad. Sci.* 111, 15332–15337.
- Schneider, C.A., Rasband, W.S., Eliceiri, K.W., 2012. NIH Image to ImageJ: 25 years of image analysis. *Nat. Methods* 9, 671–675.
- Śliwiński, M.G., Kozdon, R., Kitajima, K., Denny, A., Spicuzza, M., Valley, J.W., 2015. In-situ, micron-scale δ¹³C & δ¹⁸O analyses (by SIMS) of chemo-isotopically zoned carbonate cements of diagenetic origin—a case study on the implications for the thermal and burial history of the Eau Claire Fm., Illinois Basin (USA). In: AAPG Annual Convention and Exhibition, Denver, Colorado, 31 May–1 June (available on AAPG Search and Discovery).
- Śliwiński, M.G., Kitajima, K., Kozdon, R., Spicuzza, M.J., Fournelle, J.H., Denny, A., Valley, J.W., 2016a. Secondary ion mass spectrometry bias on isotope ratios in

- dolomite-ankerite, part I: $\delta^{18}\text{O}$ matrix effects. Geostand. Geoanal. Res. 40 (2), 157–172, <http://dx.doi.org/10.1111/j.1751-908X.2015.00364.x>, n/a-n/a.
- Śliwiński, M.G., Kitajima, K., Kozdon, R., Spicuzza, M.J., Fournelle, J.H., Denny, A., Valley, J.W., 2016b. Secondary ion mass spectrometry bias on isotope ratios in dolomite-ankerite, part II: $\delta^{13}\text{C}$ matrix effects. Geostand. Geoanal. Res. 40 (2), 173–184, <http://dx.doi.org/10.1111/j.1751-908X.2015.00380.x>.
- Śliwiński, M.G., Kozdon, R., Kitajima, K., Denny, A., Valley, J.W., 2016c. Microanalysis of carbonate cement $\delta^{18}\text{O}$ in a CO_2 -storage system seal: insights into the diagenetic history of the Eau Claire Formation (Upper Cambrian), Illinois Basin. AAPG Bull. 100, 1003–1031.
- Stevens, S.H., Pearce, J.M., Rigg, A.A.J., 2001. Natural analogs for geologic storage of CO_2 : an integrated global research program. In: Proceedings of the First National Conference on Carbon Sequestration, National Energy Technology Laboratory, Washington, DC, USA.
- Valley, J.W., Kita, N.T., 2009. In situ oxygen isotope geochemistry by ion microprobe. In: Fayek, M. (Ed.), Secondary Ion Mass Spectrometry in the Earth Sciences: Gleaning the Big Picture from a Small Spot. Mineralogical Association of Canada (MAC Shortcourse 41), pp. 19–63.
- Vermeul, V.R., Amonette, J.E., Strickland, C.E., Williams, M.D., Bonneville, A., 2016. An overview of the monitoring program design for the FutureGen 2.0 CO_2 storage site. Int. J. Greenh. Gas Control 51, 193–206, <http://dx.doi.org/10.1016/j.ijggc.2016.05.023>.
- Watson, M.N., Zwingmann, N., Lemon, N.M., 2004. The Ladbroke Grove-Katnook carbon dioxide natural laboratory: a recent CO_2 accumulation in a lithic sandstone reservoir. Energy, 6th International Conference on Greenhouse Gas Control Technologies 29, 1457–1466, <http://dx.doi.org/10.1016/j.energy.2004.03.079>.
- Wigley, T.M., Richels, R., Edmonds, J.A., 1996. Economic and environmental choices in the stabilization of atmospheric CO_2 concentrations. Nature 379, 240–243.
- Wilkinson, M., Haszeldine, R.S., Fallick, A.E., Odling, N., Stoker, S.J., Gatliiff, R.W., 2009. CO_2 -mineral reaction in a natural analogue for CO_2 storage—implications for modeling. J. Sediment. Res. 79, 486–494, <http://dx.doi.org/10.2110/jsr.2009.052>.
- Wilson, S.A., Raudsepp, M., Dipple, G.M., 2006. Verifying and quantifying carbon fixation in minerals from serpentine-rich mine tailings using the Rietveld method with X-ray powder diffraction data. Am. Mineral. 91, 1331–1341, <http://dx.doi.org/10.2138/am.2006.2058>.
- Wilson, S.A., Dipple, G.M., Power, I.M., Thom, J.M., Anderson, R.G., Raudsepp, M., Gabites, J.E., Southam, G., 2009. Carbon dioxide fixation within mine wastes of ultramafic-hosted ore deposits: examples from the Clinton Creek and Cassiar chrysotile deposits, Canada. Econ. Geol. 104, 95–112.
- Yokoulian, L.E., Freiburg, J.T., Butler, S.K., Berger, P.M., Roy, W.R., 2013. Mineralogical alterations during laboratory-scale carbon sequestration experiments for the illinois basin. Energy Procedia 37, 5601–5611, <http://dx.doi.org/10.1016/j.egypro.2013.06.482>.